CrossMark

ORIGINAL RESEARCH PAPER

# Estimates for the stiffness, strength and drift capacity of stone masonry walls based on 123 quasi-static cyclic tests reported in the literature

**Francesco Vanin**[1] · **Dario Zaganelli**[1] · **Andrea Penna**[2] ·
**Katrin Beyer**[1]

**Abstract** This paper summarises 123 existing quasi-static shear–compression tests on stone masonry walls and evaluates the results to provide the input required for the displacement-based assessment of stone masonry buildings. Based on the collected data, existing criteria for estimating lateral strength and stiffness of stone masonry walls are reviewed and improvements proposed. The drift capacity of stone masonry walls is evaluated at six different limit states that characterise the response from the onset of cracking to the collapse of the wall. To provide input data for probabilistic assessments of stone masonry buildings, not only median values but also the corresponding coefficients of variation are determined. In addition, analytical expressions that estimate the ultimate drift capacity either as a function of masonry typology and failure mode or as a function of masonry typology, shear span and axial load ratio are proposed. The paper provides also estimates of the uncertainty related to the natural variability of stone masonry by analysing repeated tests and investigates the effect of mortar injections and the effect of the loading history (monotonic vs cyclic) on stiffness, strength and drift capacities. The data set is made publicly available.

**Keywords** Stone masonry · In-plane behaviour · Drift capacity · Shear strength · Wall stiffness · Wall database

✉ Katrin Beyer
  katrin.beyer@epfl.ch

[1] Earthquake Engineering and Structural Dynamics Laboratory (EESD), École Polytechnique Fédérale de Lausanne (EPFL), School of Architecture, Civil and Environmental Engineering (ENAC), 1015 Lausanne, Switzerland

[2] Department of Civil Engineering and Architecture, European Centre for Training and Research in Earthquake Engineering, University of Pavia, Via Ferrata 1-3, 27100 Pavia, Italy

🖄 Springer

# 1 Introduction

Many buildings that are part of the European cultural heritage are stone masonry buildings. Furthermore, stone masonry construction is still used today in several developing countries. Due to the low tensile strength of the mortar and the often poor interlock between stones, stone masonry buildings are among the most vulnerable buildings when subjected to seismic loading (Grünthal 1998). Buildings with stone masonry walls can fail due to in-plane loading, out-of-plane loading or a combination of the two failure modes (Fig. 1). Out-of-plane failure modes are promoted by the large mass of stone masonry walls, the small restraint provided by timber floors and the poor interlock between the stones (D'Ayala and Speranza 2003). They are the most frequent cause for the partial or complete collapse of existing stone masonry buildings during earthquakes and their assessment is therefore of high importance (e.g. Costa et al. 2015). If out-of-plane failures are prevented by appropriate structural details such as anchors and ties, the structure can develop a global response that is governed by the in-plane behaviour of the walls and the diaphragm stiffness (Penna 2015). In-plane failure modes include the failure of piers and spandrels. While the failure of spandrels causes local failures and a global decrease in stiffness and strength, the failure of piers can lead to the collapse of the building (Beyer and Mangalathu 2012). The deformation capacity of the piers is therefore essential when assessing the ultimate limit state of stone masonry buildings.

Current codes do not distinguish between different masonry typologies when assessing the drift capacity (for a review of drift capacity models in codes, see Petry and Beyer 2014a). Eurocode 8, Part 3 (EC8-3, CEN 2005a) assigns the drift capacity based on the failure mode (shear vs flexure) and the shear span ratio $H_0/L$ where $H_0$ is the height of zero moment and $L$ the wall length:

$$\text{Shear failure:} \quad \delta_{SD} = 0.4\% \tag{1a}$$

$$\text{Flexural failure:} \quad \delta_{SD} = 0.8\% \cdot \frac{H_0}{L} \tag{1b}$$

Although the current version of EC8-3 is limited to concrete and brick masonry (CEN 2005a), due to the lack of alternative values for other masonry typologies, in engineering practice these values are often also applied to stone masonry. Equation (1) gives the drift capacities for the limit state "Significant Damage" (SD). To obtain the drift capacity at 20% strength loss (defined as near collapse limit state, NC), the drift capacities of Eq. (1a)



**Fig. 1** Stone masonry buildings after the 2009 L'Aquila earthquake that failed due to an out-of-plane mechanism (**a** photo: A. Dazio) and an in-plane mechanisms (**b** photo: A. Penna)

are multiplied by a factor 4/3 (CEN 2005a). Recent works investigated the correlation of these drift capacity models with tests on clay block masonry walls (Pfyl-Lang et al. 2011; Petry and Beyer 2014a). However, the proposed models cannot be applied directly to stone masonry since stone masonry differs from block masonry with regard to the material properties, the shape of the stones, the fabric of the masonry and the number of leaves. Kržan et al. (2015) provide on the basis of three test series minimum and maximum values of drift capacity at the SD and NC limit state but do not differentiate between different types of stone masonry.

The objective of this paper is to provide the input data for the wall limit states that is required for the probabilistic displacement-based assessment of stone masonry buildings. While the framework of probabilistic assessment procedures are established (e.g. Dolsek 2009; Vamvatsikos and Fragiadakis 2010), their application to stone masonry buildings is at the moment limited by the lack of information on the distribution of drift capacities. To provide this information, this paper evaluates median values and coefficients of variations of drifts for the following six element limit states:

- Drift at the onset of cracking $\delta_{cr}$.
- Drift at yield $\delta_y$.
- Drift limit "Significant Damage", which is defined as $\delta_{SD} = \min(3\delta_{cr}, \delta_{max})$.
- Drift at maximum force $\delta_{max}$.
- Drift at ultimate LS (20% strength drop) $\delta_u$.
- Drift at collapse (50% strength drop) $\delta_c$.

The drift at the onset of cracking is the drift for which first cracks were reported. The yield drift results from the bilinear approximation of the force–displacement response (see Sect. 2.1). The drift at maximum force $\delta_{max}$ is relevant as it marks the onset of damage concentration in few cracks (Petry and Beyer 2014b). The definition of the drift limit state "Significant Damage" is a slightly modified criterion from Tomaževič (2007). For the data set analysed here, the drift limit SD is governed in approximately half of the cases by the limit $3\delta_{cr}$ and in the other half by $\delta_{max}$. The ultimate drift $\delta_u$ is defined as the drift at which the strength has dropped to 80% of the peak strength. This is a common definition of the ultimate deformation capacity, which is used for many different structural elements and materials. The definition of collapse, on the other hand, is more subjective. Ideally, it would be related to the loss of axial load bearing capacity. Since this state was not attained by most tests, a definition related to the loss in lateral strength was chosen. It is expected that the drift at axial load bearing collapse is only marginally larger given that the strength loss is rapid and shear and axial failures strongly coupled.

To determine the probability distributions of these drift capacities and to investigate on which parameters the drift capacities depend, this paper collects the results of 123 in-situ and laboratory shear–compression tests on stone masonry walls (Sect. 2) and evaluates for theses the stiffness, the strength and drift capacities (Sects. 6–8). The analysis of the test data showed—as it had also been observed for clay block masonry walls (Petry and Beyer 2014a)—that monotonic tests lead to significantly larger drift capacities than cyclic tests while the load history has only little influence on stiffness and strength (Sect. 4). Since drift capacities are typically used for seismic assessments and therefore cyclic loads, monotonic tests are disregarded when calculating drift capacities (Sect. 8). All tests are quasi-static tests, i.e., the effect of strain rates on the response of stone masonry walls are beyond the scope of this study.

The effect of the variability of stone masonry properties on the seismic assessment of stone masonry buildings can be analysed by means of Monte-Carlo simulations, which assign each building model a different drift capacity for the stone masonry walls (Rota

et al. 2014). However, also the walls within a building have different drift capacities due to the natural variability of the stone masonry. To evaluate this aleatoric uncertainty, tests of identical wall configurations are analysed with regard to the variability of stiffness, strength and deformation capacity (Sect. 3). Seismic assessments often also investigate the effect of strengthening measures on the performance of a building. The database contains few pairs of strengthened and unstrengthened walls. The strengthening measures aim at improving the integrity of the stone masonry walls by mortar injections. Section 5 reviews pairs of unstrengthened and strengthened wall tests and computes ratios for stiffness, strength and drift capacities of strengthened to unstrengthened walls. The paper closes with a discussion of the obtained results. Based on these, future research needs are outlined that aim at improving the understanding of the various parameters that influence the in-plane properties of stone masonry walls.

## 2 Database of tests on stone masonry walls

The database contains 123 shear-compression tests on stone masonry walls from 16 test campaigns (Table 1). Collected were all shear–compression tests on stone masonry walls that were sufficiently documented in the literature. The database contains both laboratory and in-situ tests. Tests other than shear–compression tests, such as for example diagonal compression tests, were not included. All typologies of stone masonry were considered. However, test units that featured unrepresentatively few stones along the wall length were excluded (Devaux 2008). Furthermore, panels strengthened with intrusive interventions that change consistently their structural behaviour (for example, application of fibre reinforced polymers or jacketing) were not included in the database. For this reason, only tests on walls that were strengthened by injections with lime grouts were considered.

The database can be downloaded from the web repository 10.5281/zenodo.812146.[1] It comprises:

- A table with:

  - characteristic data of the test units (test campaign, type of test, geometry and masonry typology of test units, material properties, Masonry Quality Index as defined in Sect. 2.2, failure mode);
  - the bilinear approximations of the force–displacement response. The procedure for determining the bilinear approximation is outlined in Sect. 2.1;
  - drift capacities for six different limit states. The limit states were defined in Sect. 1.

- Cyclic force–displacement curves and envelopes are provided as CSV files; these were available for 110 tests. The data was digitised from the test reports using vector graphics software. For one test campaign (Magenes et al. 2010), experimental data were directly provided by the authors.

The masonry typologies of the test units in the database were classified according to the Italian code (MIT 2009), which distinguishes between five types of stone masonry:

---

[1] This database will be part of the European Masonry Database, which the authors are currently establishing in collaboration with Matija Gams (University of Ljubljana).

**Table 1** Database with shear–compression tests on stone masonry walls: list of test campaigns

| Series | References | No. of units | Masonry typology | Test type | Lab./In-situ |
|---|---|---|---|---|---|
| S1 | Vasconcelos (2005), Vasconcelos and Lourenço (2009) | 28 | E1, C | Cyclic, monotonic | Laboratory |
| S2 | Silva et al. (2014) | 16 | B | Cyclic | Laboratory |
| S3 | Mazzon (2010) | 6 | B | Cyclic | Laboratory |
| S4 | Magenes et al. (2010) | 5 | C | Cyclic | Laboratory |
| S5 | Almeida et al. (2012) | 2 | E | Cyclic | Laboratory |
| S6 | Borri et al. (2001) | 3 | A | Monotonic | In-situ |
| S7 | Borri et al. (2012) | 10 | A | Monotonic | In-situ |
| S8 | Corradi et al. (2014) | 2 | A | Monotonic | In-situ |
| S9 | Marcari et al. (2007) | 4 | D | Monotonic | Laboratory |
| S10 | Costa et al. (2011) | 1 | A | Cyclic | In-situ |
| S11 | Pinho et al. (2012) | 6 | A | Cyclic, monotonic | Laboratory |
| S12 | Lourenço et al. (2005) | 7 | E1 | Monotonic | Laboratory |
| S13 | Almeida et al. (2014) | 12 | E1, C | Cyclic | Laboratory |
| S14 | Kržan et al. (2015) | 14 | E | Cyclic | Laboratory |
| S15 | Silva et al. (2012) | 1 | C | Cyclic | Laboratory |
| S16 | Faella et al. (1992) | 6 | D | Cyclic | Laboratory |
| | Total | 123 | | | |

- Class A: irregular stone masonry, with pebbles, erratic and irregular stone units;
- Class B: uncut stone masonry, with external leaves of limited thickness and infill core (three-leaf stone masonry).
- Class C: cut stone masonry with good bond.
- Class D: soft stone regular masonry (built with tuff or sandstone blocks).
- Class E: ashlar masonry, built with sufficiently resistant blocks (i.e. blocks with higher resistance than those of class D). This class was further subdivided into regular squared block masonry with mortar joints (E) and dry-joint ashlar masonry (E1).

Typical cross-sections of these masonry typologies are shown in Fig. 2.

## 2.1 Bilinear approximation of the force–displacement curve

In shear–compression tests, the axial force is kept constant while the applied horizontal displacement is varied. The loading protocols for the horizontal displacement differed between the various campaigns and included monotonic tests and reversed cyclic tests. For the monotonic tests (35 tests, for 22 of which the load–displacement curve is available) no processing was required to obtain the envelope curve. For the reversed cyclic tests with one or three repeated cycles (24 and 57 tests, respectively), the envelope curves were derived from the digitised force–displacement hysteretic curves by connecting the points at displacement peaks. When more than one cycle was imposed per displacement amplitude, the first cycle was considered for constructing the envelope, in order to make results from different loading protocols as comparable as possible. This approach also accounts for the
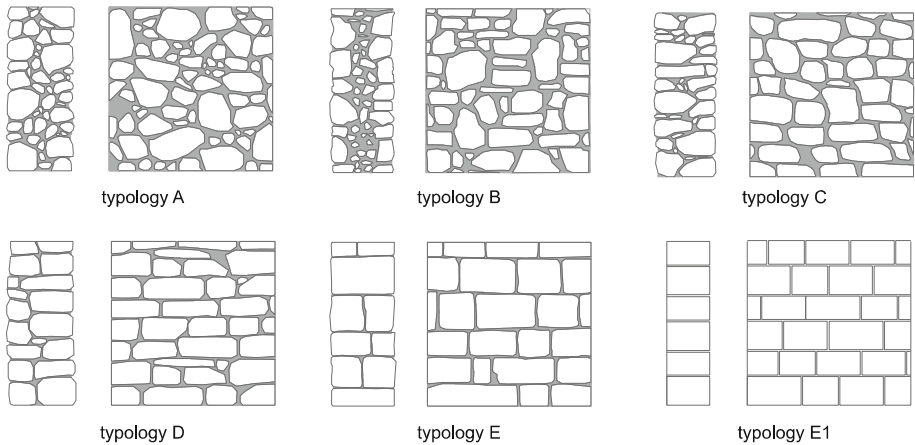
**Fig. 2** Stone masonry typologies: sketches of typical textures and cross-sections

finding that masonry piers that are part of a building, which is subjected to a real earthquake, are not likely to be subjected to more than one or two cycles at the highest drift demand (Mergos and Beyer 2014).

The bilinear approximation of the envelope curves was computed as described in Fig. 3. First, the maximum recorded strength $V_{max}$ was identified. The effective stiffness was then defined as the secant stiffness at 70% $V_{max}$. The ultimate drift $\delta_u$ was determined as the drift at which the strength had dropped to 80% $V_{max}$. If such a large drop was not attained, the largest drift that was reached during the test was taken as $\delta_u$. The ultimate strength $V_u$ was defined as the strength that yields for the bilinear approximation the same area below the curve as the actual envelope up to $\delta_u$. For cyclic tests, bilinear approximations were computed for the envelopes in the positive and negative loading direction. The final envelope curve was derived as follows: the final effective stiffness and ultimate strength correspond to the average of the values for the two directions. For the ultimate drift, however, the minimum value of the ultimate drift in the positive and negative direction was taken. When the force drop was only attained in one direction, the corresponding ultimate drift was considered for the final envelope. This procedure is similar to the one adopted by
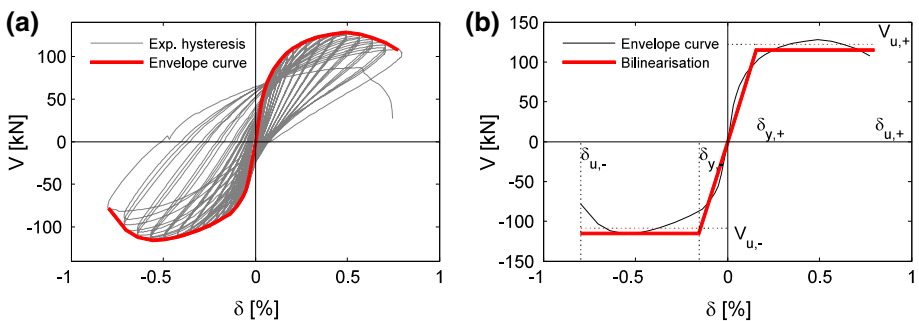


**Fig. 3** Example of a force–displacement response curve (**a**) and definition of effective stiffness, strength and drift capacity based on the envelope of the response (**b**)

Frumento et al. (2009); unlike by Frumento et al., the envelope of the first cycles was used and not the average of envelopes corresponding to repeated cycles.

## 2.2 Distribution of properties of test units contained within the database

The collected experimental data spans a wide range of test unit configurations (Fig. 4). Most tests were laboratory tests (111 test units, 90%); in addition, the database contains also 12 in-situ tests on walls that were isolated in an existing building. Of the laboratory tests, 87 (78%) were cyclic tests and 24 (22%) monotonic tests while 11 out of the 12 in-situ tests were monotonic tests and only one was a cyclic test. For nine in-situ tests and four laboratory tests only the peak force but not the complete force–displacement curve was reported (in total 13 tests, i.e., 11%). These tests could therefore only be used for the strength model but not when evaluating the stiffness and deformation capacity of the walls.
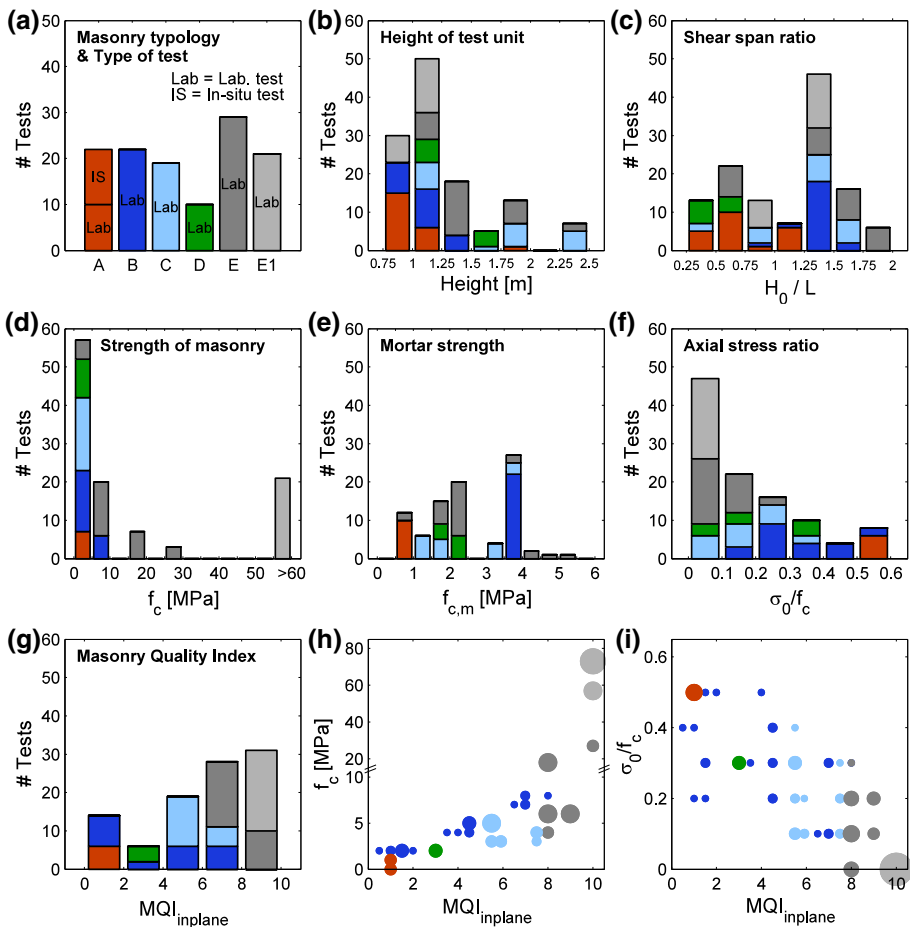


**Fig. 4** Database of shear–compression tests on stone masonry walls: distribution with regard to various parameters. The *colours* refer to the masonry typology (see plot **a**). For plots **h** and **i**, the size of the marker relates to the number of test units with the corresponding parameter combination

Figure 4a shows the number of tests that is available for each masonry typology. It further shows the portion of monotonic and cyclic tests. The colour code introduced in this figure with regard to the masonry typology is employed throughout the article. A large majority of the tests were carried out on relatively small test units with heights between 0.9 and 1.25 m and only very few tests on storey-high units (Fig. 4b). The shear span ratio $H_0/L$ varies between 0.5 and 2.0 (Fig. 4c). Most of the masonry typologies that were tested had a compressive strength less than 5 MPa while few tests of dry stone masonry (E1) had a strength larger than 50 MPa (Fig. 4d); note that the latter value was obtained from tests on masonry prisms rather than masonry walls or wallettes. The compressive strength was in 53% of the tests determined from compression tests on walls or wallettes, in 28% of the tests from prism tests; in 7% of the tests it was assumed based on code provisions (MIT 2009). In 12% of the tests, there was no information on the compression strength available and code guidelines could not be applied because a photo of the test unit was missing. The mortar strength was for all test units, for which this information was available, smaller than 6 MPa (Fig. 4e). The axial stress ratio varies between 0 and 0.6 (Fig. 4f).

To account for the individual mechanical characteristics of the stone masonry, Binda and co-workers developed a procedure for assessing the quality of the stone masonry and its compliance to the "rules of the art", which is based on a visual inspection and the evaluation of local geometric parameters (Binda et al. 2009; Cardani and Binda 2015). Based on these characteristics, Borri and co-workers developed a quantitative quality index (Borri and De Maria 2009; Borri et al. 2015), named Masonry Quality Index (MQI), which has been correlated to the masonry strength (Borri et al. 2011). It accounts for the texture of the masonry by considering the following criteria: (1) mechanical properties and conservation state of the stone units, (2) the dimensions of the stones, (3) the shape of the stones, (4) the characteristics of the wall section, including the connection of leaves, (5) the horizontality of the bed-joints, (6) the staggering of the vertical joints, (7) the quality and conservation of the mortar joints. These characteristics are evaluated largely qualitatively, according to criteria specified in Borri et al. (2015). One parameter that can be determined quantitatively is the interlock of the units, both in the in-plane and out-of-plane directions, which can be described using the concept of the length of the minimum trace (LMT), as proposed by Doglioni et al. (2009). It is defined as the minimum length of a line passing only through mortar joints, between two points that are vertically aligned and at a distance $h_v$, generally taken equal to 100 cm:

$$LMT = \frac{\text{Min. trace through joints}}{h_v} \tag{2}$$

For the test units in the database, the length of the minimum trace has been determined from photos and is tabulated in the database. The MQI assigns to each criterion a value dependent on whether the criterion is satisfied, partially satisfied or not satisfied. The resulting MQI value varies between 0 and 10. The method differentiates between the behaviour under vertical loads, out-of-plane loading and in-plane loading by assigning different coefficients to the different parameters. The MQI is evaluated for all walls that are included in the database. Figure 4g shows the distribution of the masonry quality index for in-plane loading that are obtained for the tests in the database. Masonry walls of very good quality are somewhat overrepresented in the database due to the large number of tests on walls that belong to typology E or E1. For masonry strengths smaller than 10 MPa, the MQI correlates well with the masonry compressive strength (Fig. 4g; note that this correlation does not improve if the vertical MQI is plotted). Figure 4h shows the axial load

ratio against the MQI for in-plane loading. These two quantities are not directly related. The figure shows, however, that the test designs resulted in a rather strong correlation between these two variables, i.e., the higher the MQI, the smaller was in general the applied axial load ratio. The dataset constitutes itself out of 16 different test programs that were carried out in different laboratories. As a result, the parameters were not varied in a systematic manner, which will need to be taken into account when interpreting any trends in the data. Since all walls were subjected to relatively small axial stresses in a narrow range ($\sigma_0 = 0$–2 MPa), the axial stress ratio $\sigma_0/f_c$ essentially depends on $f_c$ and therefore $\sigma_0/f_c$ varies strongly with MQI. It will therefore be difficult to distinguish between the influence of MQI and the influence of the axial stress ratio $\sigma_0/f_c$.

## 2.3 Quality control of measured peak strength

The 16 test series were performed by various research groups using different test setups, which might lead to slightly different boundary conditions. As a quality check of the applied boundary conditions, the peak strength obtained in the tests was compared to the theoretical rocking strength of an infinitely strong rigid body with the same dimensions of the masonry wall:

$$V_{rock} = \frac{NL}{2H_0} \tag{3}$$

where $N$ is the axial force, $L$ the wall length and $H_0$ the shear span. In order to compute an upper limit of the rocking strength, $N$ is taken as the sum of the applied axial load $\sigma_0 L t$ and an estimate of the self-weight of the test unit. The latter is computed assuming a specific weight of 20 kN/m$^3$ for all test units. Figure 5a shows for all test units the ratio of the ultimate strength $V_u$, which was derived from the bilinearisation of the envelope curves, to the rocking strength. Theoretically, the peak strength $V_{peak}$ of masonry walls let alone the ultimate strength $V_u$ should not be larger than $V_{rock}$. To allow for small imperfections in the applied boundary conditions, all tests with ultimate strengths less than 1.10 times $V_{rock}$ are considered when evaluating stiffness, strength and drifts in the following sections. Eight of the 123 tests do not pass this quality check and are in the following disregarded. Of the 115 retained tests, about half of the test units failed in flexure and half in shear or a hybrid mode. The distribution of the failure modes with regard to the masonry typologies are shown in Fig. 5b. For masonry typologies A and D only shear failures were observed while
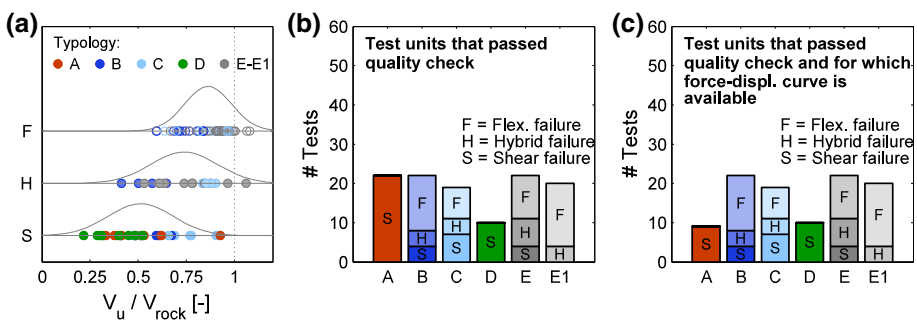


Fig. 5 Quality check of shear–compression tests on stone masonry walls: ratio of maximum shear strength to rocking strength (**a**), distribution of all tests that passed the quality check (**b**), distribution of all tests that passed the quality check and for which the force–displacement curve is available

for the other four typologies at least two out of the three failure modes were observed. Figure 5c shows the tests that passed the quality check and for which the force–displacement curve is available.

## 3 Aleatoric variability of stiffness, strength and drift limits

Stone masonry is made of the constituents stone and—unless it is dry masonry—mortar. The properties of both constituents are subject to a certain natural variability and so is the fabric of stones and mortar that is created by the mason. The properties of stone masonry walls are therefore associated with an aleatoric uncertainty, which will be estimated in the following. The data set contains 19 groups of replicate tests, i.e., groups of tests in a test series that have been conducted with the same set of parameters (Table 2). This section evaluates for each of these groups of replicate tests the variability of stiffness, strength and deformation capacity. All but one of these groups are laboratory tests; for in-situ tests only one group of replicates was available. The number of tests per group varies between 2 and 4. These group sizes are of course rather small for computing coefficients of variations. The reported values should therefore be taken as a first estimate of the scatter among replicate tests until results of replicate tests on larger groups are available.

Vasconcelos and Lourenço (2009) tested nine groups of replicates. Figure 6 shows the force–displacement curves of three groups of replicates from three different masonry typologies (C, E, E1). The plots show the positive and negative envelopes of each tests, which confirm that stiffness, strength and deformation capacity vary between the replicate tests. In the following, all 19 groups are analysed. For the tests shown in Fig. 6, the strength in the negative direction tends to be slightly larger than the strength in the positive direction indicating that there might have been a slight asymmetry in the test setup. This highlights that even replicate tests might not yield an estimate of the aleatoric variability that is related to the variability of the material properties and the fabric alone but that some variability might also be related to imprecisions of the test setup.

Table 2 summarises the coefficients of variation (CoVs) for all groups of replicates with regard to stiffness, strength and five deformation limits ($\delta_{cr}$, $\delta_y$, $\delta_{max}$, $\delta_u$, $\delta_c$). Figures 7 and 8 visualise the distributions of these CoVs by grouping the values according to failure mode and masonry typology. Only one group of replicate tests was carried out as in-situ tests. The obtained values are larger than those obtained from most laboratory tests but not larger than the maximum values obtained from laboratory tests and therefore laboratory and in-situ tests will be treated together. The CoVs of each group of replicates are plotted as a dot. In addition, for each bin the lognormal distribution fitted to these CoVs is plotted. The scatter of the CoVs is rather large but some trends can be identified. Figure 7a show the CoVs of stiffness and strength as a function of the failure mode. The CoV of the strength is slightly larger for walls that fail in shear than for walls that fail in flexure. For the stiffness, however, both failure types lead to similar CoVs.

The CoVs obtained for the drift limits $\delta_{max}$ and $\delta_u$ (Fig. 8) tend to be larger than CoVs for stiffness and strength while $\delta_{cr}$ leads to a similar CoV. All but two of the replicate groups stem from masonry typologies that have relatively regularly shaped stones and a regular bond pattern (C, D, E, E1). For typologies A and B, the stone pattern is more irregular and therefore one might expect a larger aleatoric variability. The data shows, however, that the masonry typology does not seem to have a significant influence on the aleatoric variability of the drift values. The data base for the irregular masonry typologies

**Table 2** Coefficients of variation of replicated tests for effective stiffness, strength and drift values at five limit states ($\delta_{cr}$–$\delta_u$)

| Reference | Test units | Typ. | Units | Type of test | Failure modes | CoV $K_{eff}$ | CoV $V_u$ | CoV $\delta_{cr}$ | CoV $\delta_y$ | CoV $\delta_{SD}$ | CoV $\delta_{max}$ | CoV $\delta_u$ |
|---|---|---|---|---|---|---|---|---|---|---|---|---|
| Borri et al. (2001) | B-T-04-OR, P-T-15-OR | A | 2 | In-situ | S | 0.48 | 0.16 | – | 0.34 | 0.36 | 0.36 | 0.58 |
| Pinho et al. (2012) | M5, M12, M20 | A | 3 | Lab. | S | 0.10 | 0.04 | – | 0.07 | 0.25 | 0.25 | 0.28 |
| Vasconcelos and Lourenço (2009) | WR1.100, WR2.100 | C | 2 | Lab. | F, H | 0.01 | 0.05 | 0.07 | 0.04 | 0.57 | 0.57 | 0.59 |
| Vasconcelos and Lourenço (2009) | WR1.175, WR2.175 | C | 2 | Lab. | F, H | 0.05 | 0.06 | 0.04 | 0.00 | 0.00 | 0.00 | 0.03 |
| Vasconcelos and Lourenço (2009) | WR1.250–WR3.250 | C | 3 | Lab. | S | 0.15 | 0.11 | 0.01 | 0.17 | 0.24 | 0.24 | 0.29 |
| Magenes et al. (2010) | CS00, CS02[a] | C | 2 | Lab. | F, H | 0.12 | 0.02 |  | 0.10 | 0.29 | 0.29 | 0.65 |
| Faella et al. (1992) | T1-1, T1-2, T2-1 | D | 3 | Lab. | S | 0.16 | 0.08 | 0.00 | 0.12 | 0.20 | 0.20 | 0.20 |
| Marcari et al. (2007) | P#1–P#4 | D | 4 | Lab. | S | 0.40 | 0.26 | 0.14 | 0.15 | 0.29 | 0.29 | 0.27 |
| Vasconcelos and Lourenço (2009) | WI1.100, WI2.100 | E | 2 | Lab. | F | 0.26 | 0.04 | 0.09 | 0.30 | 0.07 | 0.07 | 0.02 |
| Vasconcelos and Lourenço (2009) | WI1.175–WI3.175 | E | 3 | Lab. | F | 0.26 | 0.12 | 0.06 | 0.19 | 0.65 | 0.65 | 0.26 |
| Vasconcelos and Lourenço (2009) | WI1.250, WI2.250 | E | 2 | Lab. | F, H | 0.16 | 0.05 | 0.06 | 0.11 | 0.17 | 0.17 | 0.04 |
| Kržan et al. (2015) | Test 3–test 6[b] | E | 4 | Lab. | H | 0.69 | 0.28 | 0.16 | 0.56 | 0.40 | 0.40 | 0.28 |
| Kržan et al. (2015) | Test 7–test 10[b] | E | 4 | Lab. | S | 0.19 | 0.03 | 0.39 | 0.16 | 0.05 | 0.05 | 0.07 |
| Lourenço et al. (2005) | SW.100.1, SW.100.2 | E1 | 2 | Lab. | F, H | 0.20 | 0.07 | – | 0.13 | 0.26 | 0.26 | 0.28 |
| Lourenço et al. (2005) | SW.200.1, SW.200.2 | E1 | 2 | Lab. | H | 0.16 | 0.03 | – | 0.13 | 0.47 | 0.47 | 0.23 |
| Vasconcelos and Lourenço (2009) | WS1.100–WS4.100 | E1 | 4 | Lab. | F | 0.37 | 0.03 | 0.24 | 0.42 | 0.45 | 0.45 | 0.37 |
| Vasconcelos and Lourenço (2009) | WS1.175–WS3.175 | E1 | 3 | Lab. | F | 0.09 | 0.02 | 0.07 | 0.10 | 0.23 | 0.23 | 0.21 |

**Table 2** continued

| Reference | Test units | Typ. | Units | Type of test | Failure modes | CoV $K_{eff}$ | CoV $V_u$ | CoV $\delta_{cr}$ | CoV $\delta_y$ | CoV $\delta_{SD}$ | CoV $\delta_{max}$ | CoV $\delta_u$ |
|---|---|---|---|---|---|---|---|---|---|---|---|---|
| Vasconcelos and Lourenço (2009) | WS1.250–WS3.250 | E1 | 3 | Lab. | F | 0.04 | 0.01 | 0.05 | 0.05 | 0.20 | 0.20 | 0.20 |
| Min. | | | 2 | | | 0.01 | 0.01 | 0.00 | 0.00 | 0.00 | 0.00 | 0.02 |
| Max. | | | 4 | | | 0.69 | 0.28 | 0.39 | 0.56 | 0.65 | 0.65 | 0.65 |
| Mean | | | | | | 0.22 | 0.08 | 0.11 | 0.17 | 0.29 | 0.29 | 0.27 |
| Median | | | | | | 0.16 | 0.05 | 0.07 | 0.13 | 0.26 | 0.26 | 0.27 |
| SD | | | | | | 0.79 | 0.99 | 0.97 | 0.84 | 0.60 | 0.60 | 0.69 |

[a] Masonry strength differed between the two test units (internal information; not reported in Magenes et al. (2010))

[b] Two out of the four test units were constructed with through-stones, the other two without. Since the through-stones did not seem to influence the force–displacement response significantly, the four tests are treated as one group of replicates
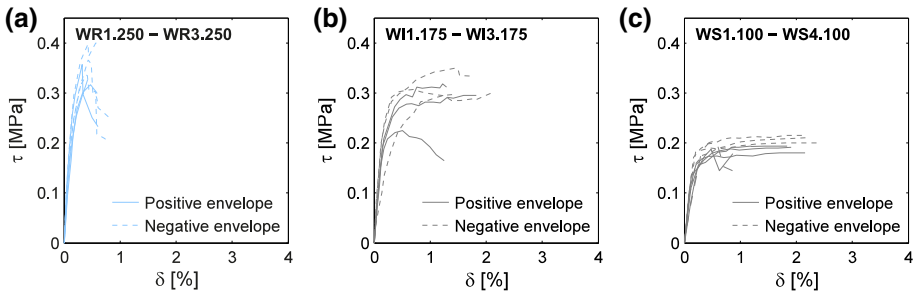
Fig. 6 Force–displacement envelopes of repeated tests by Vasconcelos and Lourenço (2009): walls of masonry typology C (a), E (b) and E1 (c)
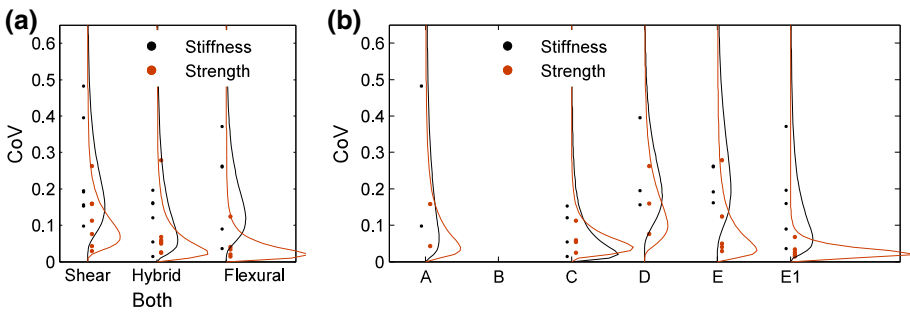


Fig. 7 Coefficients of variation of replicate tests for effective stiffness $K_{\text{eff}}$ ultimate strength $V_u$ as a function of the failure mode (a) and the masonry typology (b)
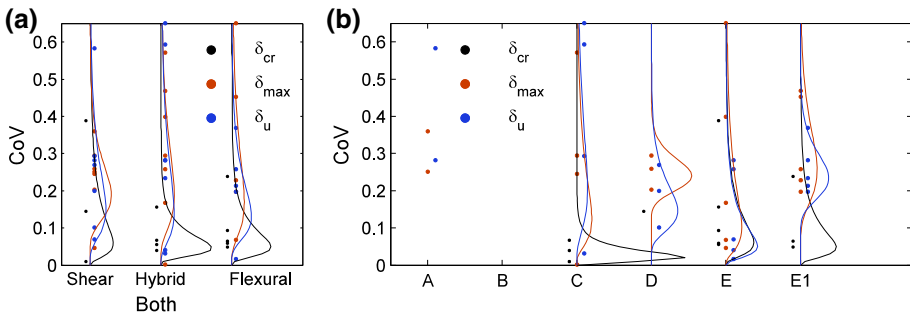


Fig. 8 Coefficients of variation of replicate tests for the drift at the onset of cracking $\delta_{\text{cr}}$, the drift at maximum strength $\delta_{\text{max}}$ and the ultimate drift $\delta_u$ as a function of the failure mode (a) and the masonry typology (b)

A and B is very scarce (A: two groups of replicate tests, B: none) and therefore the influence of the masonry typology on the aleatoric variability cannot be conclusively answered with the available data. If estimates of the aleatoric variability of stiffness, strength and deformation limits are sought for the computation of fragility curves of a class of buildings or the probabilistic seismic assessment of a specific building, it is suggested to use the values given in Table 3. These values are based on the mean values of the CoVs and rounded to the next 0.10. Note also that no test data is available for characterising the

**Table 3** Recommended values for coefficient of variations for effective stiffness, strength and drift limits

| Masonry typology and failure mode | CoV $K_{eff}$ | CoV $V_u$ | CoV $\delta_{cr}$ | CoV $\delta_y$ | CoV $\delta_{SD}$ | CoV $\delta_{max}$ | CoV $\delta_u$ | CoV $\delta_c$ |
|---|---|---|---|---|---|---|---|---|
| A–E1 | 0.20 | 0.10 | 0.10 | 0.20 | 0.30 | 0.30 | 0.30 | – |

aleatoric variability of the drift at collapse since none of the tests was continued up to a 50% drop in strength.

# 4 Effect of load history on stiffness, strength and drift limits

Among the 115 tests that passed the quality check there is only one pair of monotonic and cyclic tests (M13 and M17 by Pinho et al. 2012). Figure 9a shows the force–displacement relationships of these two tests. It shows that test units subjected to cyclic loads tend to be stiffer and exhibit a smaller drift capacity—trends that were also confirmed by tests on clay block masonry walls, for which three pairs of monotonic and cyclic tests are reported in the literature (Petry and Beyer 2014a). For clay block masonry walls, however, the strength of walls subjected to cyclic loads was similar to that subjected to monotonic loading while for the stone masonry pair the cyclic test led to a significantly larger strength than the monotonic test. At present, a systematic study on the influence of the loading history on unreinforced masonry wall response is missing. Not only a comparison of monotonic and cyclic response would be of interest, but also the influence of the number of cycles as there is evidence that most quasi-static cyclic tests on masonry walls were carried out with more cycles than what would be representative of moderate or even high seismicity (Beyer et al. 2014; Mergos and Beyer 2014).

# 5 Effect of strengthening interventions on stiffness, strength and drift limits

The dataset comprises 19 test units that were strengthened. For four of these, a non-strengthened counterpart was tested applying the same axial load and shear span (Silva et al. 2012; Silva 2012). All of these four test units were strengthened by injecting a
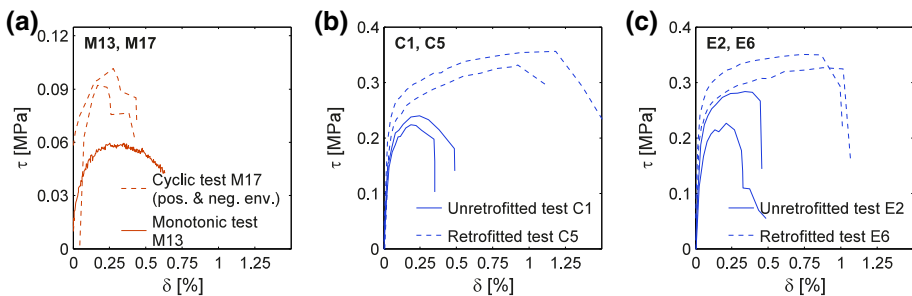


**Fig. 9** Comparison of force–displacement relationship of monotonic and cyclic tests (**a**) and strengthened and unstrengthened test units (**b**, **c**)

hydraulic lime-based grout into the voids of the wall section, which was a three-leaf wall with rubble core. The strengthening interventions were performed on the undamaged test units. Table 4 shows the ratios of properties of the strengthened to the unstrengthened test units. The number of pairs is too small to draw any statistically significant conclusions and the results are also expected to vary significantly with the retrofit intervention. The available results show that retrofitting through grout injections has the largest impact on the deformation capacity and it is particularly significant if the failure mode changes from shear to flexure. Note that while the applied axial load was the same for each pair, the axial load ratio was smaller for the strengthened specimens since their compressive strength was larger.

## 6 Stiffness of stone masonry walls

Force-based and displacement-based assessment procedures require as input an estimate of the horizontal stiffness of structural walls. The stiffness is needed to compute the dynamic properties of a building as well as its force–displacement response. The initial uncracked stiffness is only of interest in engineering practice if nonlinear structural models can account explicitly for the stiffness degradation after cracking of the element. In all other cases, i.e. for simplified structural models (bilinear models for each structural element) or force-based assessment procedures, the effective stiffness is of interest. However, in the absence of better models, current codes suggest to estimate the effective stiffness as a ratio of the elastic uncracked stiffness (e.g. CEN 2005b) which, therefore, should be determined with sufficient accuracy.

**Table 4** Pairs of strengthened and unstrengthened test units: ratio of properties of strengthened to unstrengthened test unit

| Reference | Labels of unstrengthened and strengthened test units | | Typ. | Failure mode of unstrengthened and strengthened test units | | Intervention | Ratio of properties of strengthened to unstrengthened test unit | | | | | |
|---|---|---|---|---|---|---|---|---|---|---|---|---|
| | Unstr. | Str. | | Unstr. | Str. | | $f_c$ | $K_{eff}$ | $V_u$ | $\delta_{cr}$ | $\delta_{max}$ | $\delta_u$ |
| Silva (2012) | C1 | C5 | B | Shear | Flex. | Injected | 1.7 | 0.8 | 1.5 | 3.5 | 6.3 | 4.3 |
| Silva (2012) | C2 | C7 | B | Shear | Flex. | Injected | 1.7 | 1.7 | 2.0 | 2.6 | 5.8 | 6.2 |
| Silva (2012) | E2 | E6 | B | Flex. | Flex. | Injected | 2.0 | 1.5 | 1.3 | 1.9 | 3.5 | 3.2 |
| Silva (2012) | E4 | E5 | B | Flex. | Flex. | Injected | 2.0 | 1.0 | 1.4 | 1.8 | 2.5 | 2.6 |
| Mean values | | | | Shear | Flex. | | 1.7 | 1.3 | 1.8 | 3.0 | 6.0 | 5.3 |
| Mean values | | | | Flex. | Flex. | | 2.0 | 1.3 | 1.3 | 1.8 | 3.0 | 2.9 |
| Italian code | | | | | | | | | | | | |
| Ratios for typology B (MIT 2009) | | | | | | Injected | 1.7 | 1.7 | 1.7 | – | – | – |

This section computes from the force–displacement envelopes the ratio of effective to uncracked stiffness and compares the obtained values to code estimates (Sect. 6.1). The remainder of the section evaluates different methods of estimating the E-modulus. First, the median values and CoVs of the E-modulus are computed for the various masonry typologies (Sect. 6.2). Second, the E-modulus is computed from results of compression tests and dynamic identification tests that were carried out as part of the experimental campaigns (Sect. 6.3). The so obtained E-moduli are applied to compute the horizontal stiffness of the walls and conclusions are drawn on which kind of tests are suitable for obtaining estimates of E-moduli. When assessing a masonry building, in-situ tests to determine the elastic properties, such as flat-jack tests, are often not available and their use can be questionable for multiple-leaf stone masonry. It can be necessary, hence, to estimate the E-modulus from the compressive strength of the masonry, which is often the first material parameter that is determined from tests or assumed based on code values. Section 6.4 proposes such an expression, which also accounts for the effect of the axial load ratio on the effective stiffness. The last section compares the different approaches for estimating the stiffness with regard to the bias and coefficient of variations (Sect. 6.5).

## 6.1 Ratio of effective to uncracked stiffness

Current codes estimate the effective stiffness postulating a constant ratio between initial uncracked stiffness and effective stiffness; EC8-3 recommends a ratio of 0.5 (CEN 2005b) and the Swiss guidelines SIA D0237 a ratio of 0.3 (Pfyl-Lang et al. 2011). To check the applicability of these assumptions, the experimental initial uncracked stiffness was calculated from the envelopes as the secant stiffness at 15% of the maximum force; for cyclic tests, the average of the stiffness derived from the positive and negative envelopes is considered. Similarly, the effective stiffness was defined as the secant stiffness at 70% of the maximum force. Figure 10a shows the ratios of effective to elastic stiffness that were obtained from the wall tests. The variation is rather large for all failure modes and slightly larger for walls failing in shear or a hybrid mode than for walls failing in flexure. Clear differences between masonry typologies could not be identified. Table 5 summarises the experimentally determined ratios; despite the large uncertainty, a value of 0.5, as suggested by EC8, is close to a mean estimate for all failure modes.
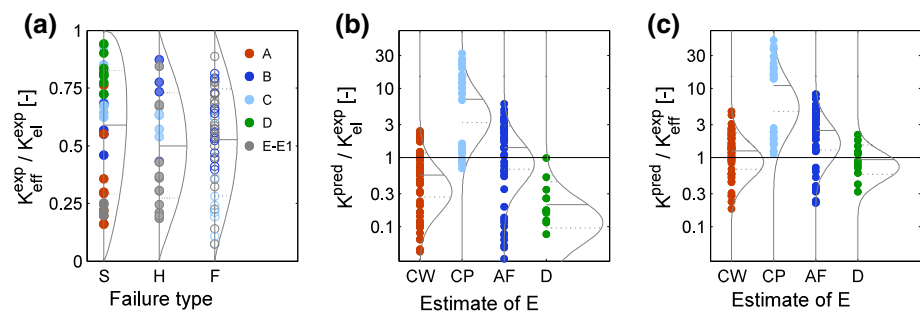


**Fig. 10** Stiffness of walls subjected to horizontal loads: effective to elastic wall stiffness ratios for different failure types and masonry typologies (**a**); estimate of the experimental elastic wall stiffness (**b**) and effective wall stiffness (**c**) from different types of tests (*CW* compression tests on walls; *CP* compression tests on prisms; *AF* stiffness measured when applying the axial force at the beginning of the shear–compression test; *D* dynamic identification tests)

**Table 5** Experimental determination of effective to elastic stiffness ratio

| Experimental ratio of effective to elastic stiffness | Experimental failure mode | | |
|---|---|---|---|
| | Shear | Hybrid | Flexure |
| Average $K_{eff}^{exp}/K_{el}^{exp}$ | 0.59 | 0.50 | 0.53 |
| CoV | 0.51 | 0.45 | 0.41 |

## 6.2 E-modulus as a function of the masonry typology

For all tests, for which the force–displacement curve was reported, the E-modulus of the masonry can be back-calculated from the horizontal stiffness of the wall. Generally, the stiffness of masonry walls is computed by means of Timoshenko beam models, which account for both flexural and shear deformability with the latter being particularly relevant for the typical slenderness ratios of masonry piers. Applying the Timoshenko beam theory, the elastic stiffness $K_{el}$ of a wall with a rectangular cross section and a height $H$ and shear span $H_0$ that is subjected to a horizontal force at its top is:

$$K_{el} = \frac{1}{\frac{H^3}{2EI}\left(\frac{H_0}{H} - \frac{1}{3}\right) + \frac{6H}{5GLt}} \tag{4}$$

where $E$ and $G$ are the Young modulus and the shear modulus of the masonry, which is idealised as a homogeneous continuum. For back-calculating the E-modulus from the measured stiffness, it was necessary to assume a ratio of the G- to E-modulus. Eurocode 6 (CEN 2005b) recommends a ratio $G/E$ of 0.4 for all types of masonry if a better estimate is not available. Much lower $G/E$-ratios, in the range 0.06–0.25, are reported in the literature (e.g. Tomaževič 1999). According to the elasticity theory of homogenous isotropic materials the maximum Poisson ratio is 0.5 and therefore the minimum $G/E$-ratio 0.33. Considering the composite anisotropic nature of the masonry material, smaller $G/E$-ratios are, however, possible. The Italian code (MIT 2009) assumes for most stone masonry typologies a ratio of $G/E$ equal to 0.33 and this ratio was also adopted here. Based on this assumption, the E-modulus can be computed from the experimental stiffness of the wall:

$$E_{exp} = K_{exp} \frac{6/5H \cdot \left[1 + 5\left(H_0/H - 1/3\right) \cdot G/E \cdot \left(\frac{H}{L}\right)^2\right]}{G/E \cdot Lt} \tag{5}$$

Average values of the elastic and the effective stiffness and standard deviations derived for each masonry typology are reported in Table 6. The effective stiffness values are compared to the ranges indicated by the Italian code in Fig. 12a. For typologies A, C and D the reference values proposed in the Italian code provide a reasonable estimate in terms of mean values, while the error of the predicted stiffness is considerable for the other typologies. In order to make the code ranges representative of 16th–84th fractiles of a probability distribution, as suggested in CNR (2013), the variance of the stiffness should be significantly increased for all stone masonry typologies. However, if one considers the modification factors proposed in the code for considering various mortar qualities, the code ranges for stiffness and strength would be enlarged and the variance of the distribution, therefore, increased. Nonetheless, given that a large part of the tests considered for this

**Table 6** Elastic and effective stiffness ranges for the various masonry typologies

| | Masonry typology | | | | | |
| --- | --- | --- | --- | --- | --- | --- |
| | A | B | C | D | E | E1 |
| Italian code[a], $E_{el}$ (MPa) | 870 | 1230 | 1740 | 1080 | 2800 | 2800 |
| CoV | 0.21 | 0.17 | 0.14 | 0.17 | 0.14 | 0.14 |
| Italian code[a], $G_{el}$ (MPa) | 290 | 410 | 580 | 360 | 860 | 860 |
| CoV | 0.21 | 0.17 | 0.14 | 0.17 | 0.09 | 0.09 |
| Number of tests | 10 | 7 | 18 | 10 | 20 | 22 |
| Elastic stiffness, $E_{el}$ | | | | | | |
| Median (MPa) | 1110 | (3650)[b] | 1900 | 510 | 1460 | 1000 |
| CoV | 0.63 | (0.39)[b] | 0.69 | 0.48 | 0.61 | 0.43 |
| Effective stiffness, $E_{eff}$ | | | | | | |
| Median (MPa) | 320 | (2240)[b] | 900 | 430 | 550 | 630 |
| CoV | 0.49 | (0.22)[b] | 0.38 | 0.42 | 0.57 | 0.42 |
| $\left(E_{eff}/f_c\right)_{ref}$ | 400 | (700)[b] | 300 | 250 | 200 | 250 |

[a] The Italian code (MIT 2009) gives an upper and lower bound value. According to CNR (2013), they be interpreted as the 16th and 84th percentile values. The mean value given here is computed as the average of the upper and lower bound value and the CoV, assuming a lognormal distribution, as $\sqrt{e^{\beta^2}-1}$, where $\beta$ is the logarithmic standard deviation computed as $1/2(\ln E_{84\%} - \ln E_{16\%})$

[b] The values of stiffness for typology B are derived from a single test campaign

study are laboratory tests on panels built with good quality mortar, the variability of the stiffness and strength properties seems to be related to an aleatoric variability rather than to the quality of the materials.

## 6.3 Determining the E-modulus from compression tests or dynamic identification tests

Most test campaigns with shear–compression tests on stone masonry walls also comprised some material tests from which the elastic properties of the masonry can be estimated. Different types of tests were carried out for this purpose. Most common are compression tests on wallets or masonry prisms. The wallets had typically dimensions of approximately 1 m by 1 m while the prisms were much smaller and comprised just a vertical stack of 3–5 stones. In addition to compression tests, some research groups determined the elastic properties from dynamic identification tests or from the deformation measured when applying the vertical load to the wall. The G-modulus is more difficult to determine than the E-modulus, and test reports do often not report estimates for the G-modulus and such values are therefore also not included in the database.

Figure 10b, c show the distributions of errors in predicting the elastic and effective wall stiffness when determining the E-modulus from compression tests on wallets (CW), compression tests on prisms (P), from deformations measured when applying the axial force at the beginning of the shear–compression tests (AF) and from dynamic identification tests (D) on the walls that are later used for shear–compression tests. The estimate of the effective stiffness is in general characterised by a smaller dispersion, compared to the elastic stiffness. The results show that the elastic properties should not be derived from compression tests on prisms (Lourenço 1996; Oliveira 2003), but that the compression tests

should be carried out on wallets. Compression tests on prisms tend to overestimate the E-modulus, most likely because the texture of prisms is typically much more uniform than that of larger masonry walls.

As presented in more detail in Fig. 11, the test that leads to the smallest bias and uncertainty is the compression test on masonry wallets and this is therefore the preferred test for estimating the E-modulus. The stiffness derived from the axial force load stage is affected by a larger uncertainty than compression tests on masonry wallets, most likely because the walls are only loaded to relatively small axial load ratios where the stress–strain relationship can be nonlinear. Dynamic identification tests were used only for few tests and therefore conclusions on the reliability of the properties obtained from such tests cannot be derived.

Based on the three more reliable estimates of the elastic properties—compression tests on walls, axial force load stage, dynamic identification tests—the effective stiffness can be estimated by assuming a ratio of effective to elastic stiffness and a $G/E$-ratio. Figure 10 shows the distribution of the errors of predicted effective stiffness if one assumes for all typologies and failure modes a ratio of effective to elastic stiffness equal to 0.5 and the ratio of $G/E$ as 0.33. Standard deviations of the errors are in general smaller than for the elastic stiffness (Table 6); this might be related to the fact that the effective stiffness is a more robust measure when determined from experimental envelopes than the elastic stiffness.

## 6.4 Determining the E-modulus from the compression strength

In engineering practice, compression or dynamic identification tests can often not be conducted and reference values have to be obtained from the literature or from code provisions. Many codes only tabulate the compressive strength and estimate the E-modulus as $1000 f_c$, a value suggested also by Eurocode 6 (CEN 2005b). However, such ratio has been shown to be highly variable when determined from experimental tests, as pointed out by Tomaževič (1999), who reported for this ratio values between 200 and 2000. On average, in the collected sample of tests, the ratio between the experimental effective stiffness and the compressive strength of masonry tends to increase with the axial load ratio, as shown in Fig. 12b. An increase of the effective stiffness with applied axial load had already been reported by a few authors (Vasconcelos 2005; Bosiljkov et al. 2005). However, not all test campaigns show a clear trend in this regard (for example, Magenes
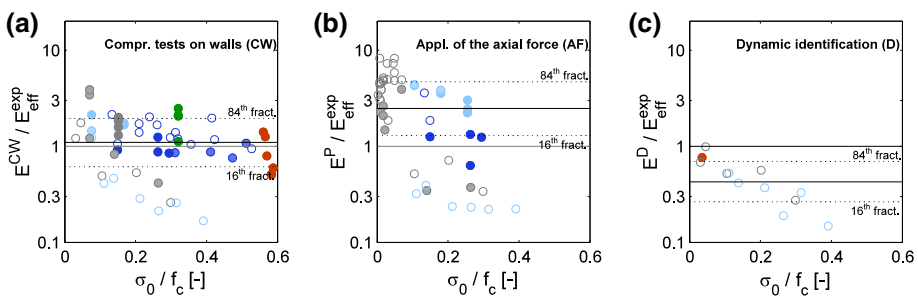


Fig. 11 Estimate of the effective stiffness for different experimental test: compression test on walls (a), stiffness measured during the application of the axial force before the shear–compression test (b), and dynamic identification tests (c)

et al. 2010). Assuming that an increase of stiffness is related to the axial load ratio, the experimental effective stiffness can be estimated through an empirical relation of the type:

$$E_{eff} = \left(\frac{E}{f_c}\right)_{ref} \cdot f_c \cdot \frac{\sigma_0/f_c}{0.30} \tag{6}$$

This simple linear formula has limits when applied to axial stresses close to zero. However, the available data and the significant scatter did not justify a more complex relationship between stiffness and axial load ratio (Fig. 12b). Reference values of the expected ratio between effective stiffness and compressive strength refer to an axial load ratio of 30%. They are derived from the database and are tabulated for the various typologies in Table 6. The ratio of experimental stiffness to the stiffness predicted by Eq. (6) is shown in Fig. 12c.

## 6.5 Comparison of various approaches for estimating the stiffness

The accuracy of the various approaches for estimating the effective stiffness is compared in Table 7. Estimating the effective stiffness from E-moduli that were determined experimentally from compression tests on walls or prisms, dynamic identification tests or computed from the shortening of the wall when applying the axial load leads to large uncertainties (CoV = 0.5–0.7) and considerable bias. Surprisingly none of these results led to an improved estimate of the horizontal wall stiffness when compared to the Italian code values.

The use of median values of $E_{eff}$ obtained from the collected tests reduces obviously the bias but not much the coefficient of variation. Moreover, it should be considered that in Fig. 12 and in Table 6 typology B represents solely unstrengthened panels, which are derived from a single test campaign, hence their use for assessment is not recommended but a larger number of tests from different campaigns would be required to derive reliable reference values. Strengthened panels were excluded from the sample relative to typology B since their elastic properties are significantly affected by the intervention, and they are therefore not directly comparable to the unstrengthened ones. The formulation in Eq. (6), with the reference parameters calibrated on the collected sample of tests, can reduce both the bias and the coefficient of variation of the estimate of the stiffness. In this case strengthened panels were also included in the analysis, since the ratio between elastic
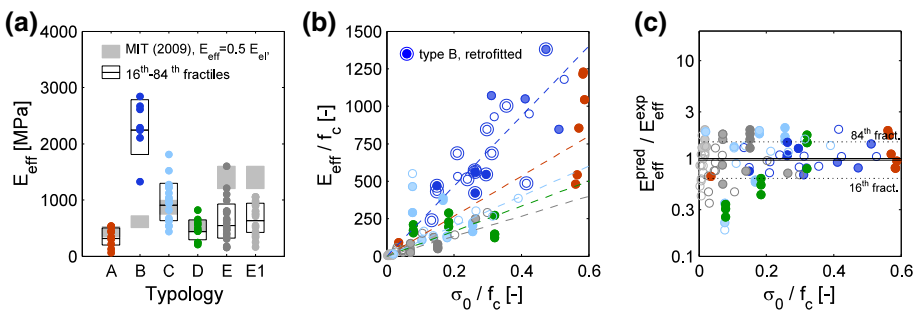


Fig. 12  a Comparison between the experimental effective stiffness and the ranges proposed in the Italian code; b relation between effective stiffness and axial load, normalized to the compressive strength $f_c$; c prediction of the effective stiffness through Eq. (6)

**Table 7** Comparison of different methods for estimating the effective stiffness of the shear–compression tests

| | Compression test, walls (CW) | Compression test, prisms (CP) | Axial force application (AF) | Dynamic identification (D) | MIT (2009), mean values | Experimental median values (Table 6) | Equation (6) (Table 6) |
|---|---|---|---|---|---|---|---|
| Number of tests | 57 | 34 | 49 | 12 | 84 | 84 | 99 |
| $E^{pred}/E^{exp}_{eff}$, median | 1.25 | 11.1 | 2.46 | 0.93 | 1.31 | 1.00 | 0.92 |
| CoV | 0.67 | 1.06 | 0.73 | 0.52 | 0.91 | 0.69 | 0.45 |

modulus and compressive strength, which is the main parameter of the formulation, does not appear to be strongly affected by the intervention (Fig. 12b).

# 7 Strength of stone masonry walls

The in-plane shear force capacity of stone masonry walls is typically evaluated from equations that model the different failure modes of the wall, namely rocking failure with crushing of the compressed toe and shear failure with diagonal cracking or sliding along the bed joints (Magenes and Calvi 1997). Expressions to evaluate the strength capacity relative to these different failure modes are available in the literature and in the codes (CEN 2005a; MIT 2009).

## 7.1 Strength equations in Eurocode 8, Part 3

The force capacity of a pier failing in flexure can be evaluated neglecting the tensile strength given that the tensile strength of masonry is normally very small and that horizontal cracking due to cyclic loading is expected at ultimate limit state. Eurocode 8, Part 3 (EC8-3) computes the flexural strength as follows:

$$V_{fl} = \frac{L^2 t}{2H_0} \sigma_{0,tot} \left( 1 - \frac{1}{\kappa} \frac{\sigma_{0,tot}}{f_c} \right) \tag{7}$$

where $\sigma_{0,\text{tot}}$ is the mean vertical stress acting at the base of the pier and $f_c$ is the compressive strength of masonry. EC8-sets the factor $1/\kappa$ equal to 1.15, which corresponds to a rectangular stress block in which the maximum stress is equal to $\kappa f_c = 0.87 f_c$. A linear stress distribution at the wall toe would lead to a factor $1/\kappa = 1.33$, while a value equal to 0 can be assumed if the compressive strength is considered infinite, for which the expression in Eq. (7) is equivalent to the rocking capacity in Eq. (3). For assessment purposes, EC8-3 suggests to use design values for $f_c$ that are multiplied by a confidence factor to account for the uncertainty, which depends on the knowledge that is available on that particular structure. However, for the scope of this study, no confidence factor is applied and the compressive strength derived from compression tests are employed.

Shear failure is modelled by EC8-3 by means of a Mohr–Coulomb criterion to be applied to the portion of the wall that is subjected to compression stresses. Although EC8-3 refers only to brick or concrete block masonry, the application of the approach was checked also for stone masonry walls. This criterion is meant to describe failure due to the interaction of flexural cracking and shear at the base of a masonry pier. The uncracked length of the wall $L_c$ can be estimated adopting a suitable stress distribution and considering the axial force acting at the base of the wall. If the tensile strength is disregarded and a triangular stress distribution is adopted, one can write the Mohr–Coulomb criterion as follows:

$$V_{MC} = L_c t c + \mu L t \sigma_{0,tot} = Lt \left( \frac{3/2 c + \mu \sigma_{0,tot}}{1 + 3 cH_0 / \sigma_{0,tot} L} \right) \tag{8}$$

where $c$ and $\mu$ are the cohesion and the friction coefficient of masonry. The parameters $c$ and $\mu$ should be interpreted as global strength parameters and should not be derived directly from interface tests on joint interfaces, in order to account for the non-uniform

stress distribution along the compression zone. EC8-3 indicates for the friction coefficient a value equal to 0.4, while reference values for the cohesive contribution in stone masonry walls should be assumed from the literature. As an additional condition accounting indirectly for tensile cracking in the units, EC8-3 prescribes that the average shear stress in the uncracked length of the wall should be less than the 6.5% of the compressive strength of the units. However, this latter criterion is meant to be applied to brick/block masonry to account for possible shear cracking through the units. In the case of stone masonry piers, due to the typically high strength of stone units, this condition is seldom the governing criterion and alternative formulations should be used to consider the possible activation of shear failures involving sub-diagonal cracking (e.g. Turnšek and Čačovič).

## 7.2 Application of strength equations to database

The criteria proposed in EC8-3 (CEN 2005a) were applied to the tests collected in the database and the effectiveness of standard code formulations in predicting correctly the experimental failure mode and force capacity was evaluated. Mechanical properties documented in the test reports do not include the shear strength parameters $c$ and $\mu$. The friction coefficient value suggested in EC8-3 is applied ($\mu = 0.4$). The cohesion was estimated assuming a parabolic tension cut-off as $c = 2\mu f_t$, where the tensile strength $f_t$ can be derived from code provisions (MIT 2009). The force capacity is defined as the ultimate shear capacity derived from the bilinear idealisation of the envelope curves. For 15 tests, the load displacement curve is not available and the maximum force capacity reported by the authors was used instead. The average ratio of maximum to ultimate force capacities is 1.04, and it exceeds the value 1.10 in less than 2% of the cases. The failure mode that was attributed to each test is based on the information provided in test reports, which assess the failure modes based on the observed damage (diagonal or horizontal cracking, sliding, crushing at the toe). However, this attribution can be somehow subjective, and mixed or hybrid failure modes are frequently observed.

EC8-3 predicts the failure mode based on the force capacities computed for flexural and shear failure: the smaller force capacity is assumed to control the failure mode. Figure 13a compares the experimentally observed failure mode to the failure mode predicted by EC8-3. The failure mode is well predicted for walls failing in flexure. For some walls failing in shear, EC8-3 predicts also a flexural failure. However, this does not necessarily mean that the prediction of the force capacity is wrong, since also walls developing large shear cracks might fail due to the crushing of the compressed corner. Moreover, shear and flexural capacity equations might lead to rather similar results and while the failure mode might be incorrectly predicted the shear strength might be rather well estimated. An incorrect prediction of the failure mode can have, however, a significant influence on the estimate of the deformation capacity. Most of today's codes assign the displacement capacity based on the failure mode and assume that walls failing in flexure have roughly twice the displacement capacity of walls failing in shear. The fact that a part of the observed shear and hybrid failures are predicted to be flexural failures might therefore lead to unconservative estimates of the deformation capacity (see next section).

For flexure-dominated walls the prediction of the force capacity is fairly good (Fig. 13b), since it depends mainly on geometrical dimensions and loading conditions, and only to a minor extent on material properties. The ratio of predicted to experimental force capacity, for flexural walls, has a median of 0.93 and a coefficient of variation (CoV) of 15%. The prediction is less accurate for higher axial load ratios, indicating that the assumption of a stress block with $\kappa = 0.87$ at the corner of the wall is probably rather
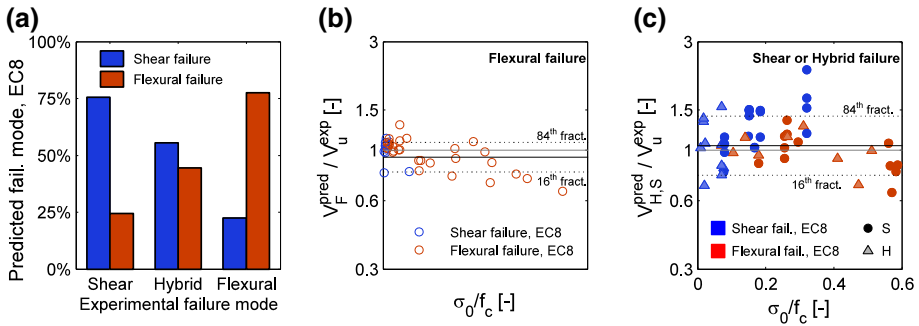
**Fig. 13** **a** Failure mode predicted by Eurocode 8 Part 3; **b** estimate of the flexural capacity; **c** estimate of the shear capacity according to EC8-3 (Mohr–Coulomb criterion on the uncracked length of the section)

conservative. The best prediction of the force capacity, with a mean of 1.00 and a CoV of 12%, is obtained for $\kappa = 1.20$, which would correspond to a local increase of the compressive strength at the base of the wall. A physical justification of this could be the presence of relatively large stones in the wall corners, which increase local strength properties. For brick masonry, also a confinement of the lowest brick row due to the foundation was observed (Petry and Beyer 2015). However, the refinement of the assumptions with regard to the stress block does not seem warranted, as the shift of the predicted force capacity is rather small and the coefficient of variation does not reduce consistently.

The predicted force capacity of walls showing hybrid or shear failure is affected by a larger uncertainty, related primarily to the estimation of the mechanical parameters, which play for these failure modes a significant role. The force capacity is on average overestimated, in a more evident manner for walls subjected to high axial load ratios (Fig. 13c). This can be related to the assumptions on the friction coefficient, for which a value of 0.4 is adopted in the Eurocode, regardless of the type of masonry. Angelillo et al. (2014) indicate different reference values for stone masonry, ranging from 0.2 for rubble masonry, 0.3 for irregular masonry, to 0.4 for dry joints stone masonry.

If a Mohr–Coulomb formulation is adopted for the assessment of the shear capacity, results are strongly affected by the choice of a suitable value for the friction coefficient. In this study, the cohesive term was assumed to be dependent on the tensile strength, which was derived from code provisions. The friction coefficient, and the uncertainty related to its determination, were hence derived from a linear regression, as shown in Fig. 14c. Only panels showing shear or hybrid failure modes were considered. Depending on the masonry typology, the so obtained friction coefficient varies between 0.2 and 0.4 (Table 8).

The mean values and coefficient of variation of the ratio of predicted to experimental force capacity for the different material properties and models for shear capacity are summarised in Table 9.

### 7.3 Turnšek–Čačovič criteria and calibration of the tensile strength

The Mohr–Coulomb criterion in EC8-3 is suitable for cases in which shear failure is associated with bed joint sliding and the opening of head joints. For irregular masonry typologies, however, the physical significance of such criterion can be questionable. An alternative formulation, proposed originally by Turnšek and Čačovič (1971), relates the
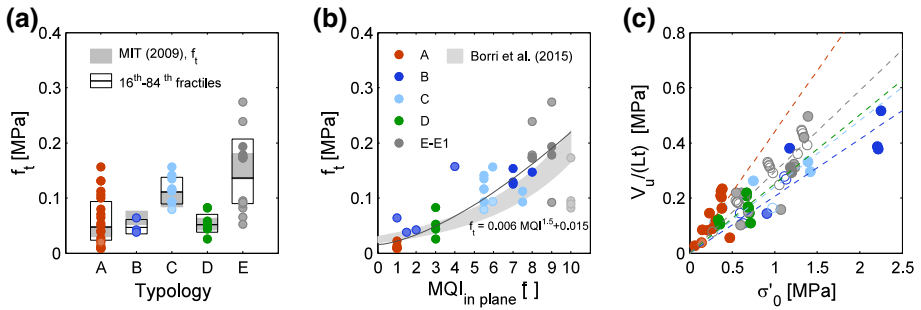
Fig. 14 a Masonry tensile strength according to Turnšek–Čačovič criterion: comparison with ranges suggested in the Italian code (MIT 2009); b estimate of the experimental tensile strength from the Masonry Quality Index; c regression analysis for the estimation of the friction coefficient; the cohesive contribution is subtracted, assuming $c = 2\mu f_t$. The x-axis is derived from Eq. (8): $\sigma'_0 = \sigma_0 + 3f_t - 6^{VH_0 f_t}/_{\sigma_0 L^2 t}$ where $V_u = \mu \cdot \sigma'_0 \cdot Lt$

Table 8 Experimental and code ranges for the tensile strength of masonry $f_t$

| | Masonry typology | | | | |
|---|---|---|---|---|---|
| | A | B | C | D | E-E1 |
| Italian code MIT (2009a)[a], $f_c$ (MPa) | 1.40 | 2.50 | 3.20 | 1.90 | 7.00 |
| CoV | 0.30 | 0.20 | 0.19 | 0.27 | 0.14 |
| Italian code MIT (2009a)[a], $f_t$ (MPa) | 0.039 | 0.065 | 0.098 | 0.053 | 0.158 |
| CoV | 0.24 | 0.19 | 0.14 | 0.20 | 0.14 |
| Experimental $f_t$ | | | | | |
| Median (MPa) | 0.047 | 0.046 | 0.111 | 0.052 | 0.136 |
| CoV | 0.79 | 0.29 | 0.22 | 0.32 | 0.44 |
| Friction coefficient, experimental | | | | | |
| Best fit | 0.44 | 0.21 | 0.24 | 0.25 | 0.29 |
| CoV | 0.17 | 0.12 | 0.17 | 0.12 | 0.04 |

[a] Mean values and coefficients of variation calculated as in Table 6

shear force capacity to the onset of diagonal cracking. The opening of a diagonal crack can be modelled through a tensile criterion, applied to an idealised biaxial stress condition in the middle of the masonry panel, obtaining the formulation in Eq. (9).

$$V_{TC} = \frac{Lt}{b} f_t \sqrt{1 + \frac{\sigma_{0,mid}}{f_t}} \qquad (9)$$

The vertical stress $\sigma_{0,mid}$ is the mean vertical stress at the mid-height of the panel, since it is assumed that diagonal cracking initiates there. The factor $b$ models the distribution of shear stresses along a horizontal section of the wall and corresponds to 1.5 if a parabolic shear stress distribution is assumed. For squat panels, however, this idealisation can be rather crude and a value of $b = HL$ ($1.0 \leq b \leq 1.5$) was found to be more appropriate (Benedetti and Tomaževič 1984). The parameter $f_t$ represents the tensile strength of masonry along an inclined plane, and can be determined from diagonal compression tests.

**Table 9** Estimation of force capacity through different models, for walls showing hybrid and shear failure

| | EC8-3 $\mu = 0.4$, $c$ from MIT (2009a)[a] | EC8-3 $\mu$ from Table 9, $c$ from MIT (2009a)[a] | Equation (9) $f_t$ from MIT (2009a)[a] | Equation (9) typology median $f_t$ | Equation (9) $f_t$, from Eq. (11) |
|---|---|---|---|---|---|
| $V^{pred}/V^{exp}$, median | 1.04 | 0.88 | 1.04 | 0.95 | 0.94 |
| CoV | 0.31 | 0.26 | 0.22 | 0.18 | 0.24 |
| Predicted to fail in shear[b] (%) | 72 | 85 | 77 | 80 | 76 |

[a]   Table C8A.2.1 in (MIT 2009). Correction coefficients in table C8A.2.2 in (MIT 2009) to account for the effect of grout injections and quality of mortar

[b]   Ratio of walls predicted to fail in shear to walls that experimentally showed shear failure

The Italian code, which suggests this equation for irregular masonry or for walls built with weak units, provides also reference values for $f_t$.

If the failure criterion expressed in Eq. (9) is adopted for all tests with hybrid or shear failure modes, one experimental value of tensile strength can be derived for each test using Eq. (10).

$$f_t = -\frac{\sigma_0}{2} + \sqrt{\left(\frac{\sigma_0}{2}\right)^2 + \left(\frac{b \cdot V_u}{Lt}\right)^2} \tag{10}$$

Figure 14a shows the comparison of ranges proposed in the Italian code for the tensile strength of masonry for the different typologies, with the values estimated from the collected tests. The obtained mean values are comparable—though typically slightly higher—than the values included in the Italian code. It should be noted that typology B refers to unstrengthened conditions. The values listed in Table 8 derive from a single test campaign and a limited number of tests, since the majority of collected tests of the same typology was strengthened through grout injections. Similarly to what was found for the effective stiffness, the code ranges do not appear currently suitable to represent 16th–84th fractiles of a probability distribution of the measure. The code ranges shown in Fig. 14a do not include the correction factors that are proposed by the Italian code to consider that the mortar of the test units tested in laboratory conditions was most likely good quality mortar, often containing hydraulic lime. The quality of the mortar present in existing buildings can be considerably lower, since its composition and conservation state might differ significantly to the ones of mortars tested in the laboratory. Therefore, depending on the state of the mortar, the adoption of conservative values for assessment purposes can be advisable. An alternative method for estimating the tensile strength of an existing stone masonry could make use of the Masonry Quality Index (MQI). In Fig. 14b the experimental values of tensile strength are related to the MQI estimated for each panel, evaluated for in-plane actions. A regression of experimental values through a simple equation can be expressed as:

$$f_t = 0.015 + 0.006 \cdot MQI^{1.5} \tag{11}$$

Equivalent expressions that link upper and lower bounds of the tensile strength to the MQI were developed by Borri et al. (2015). These expressions, although their form is slightly different, show the same trend and lead to similar estimates of the tensile strength.

### 7.4 Comparison of different strength models

A comparison of the different capacity models for the prediction of the lateral strength of panels showing hybrid or shear failure modes are summarised in Table 9. In general, the application of a Turnšek–Čačovič failure criterion improves the prediction of the force capacity when compared to the standard approach prescribed in EC8-3. This applies to both approaches of estimating $f_t$, i.e., estimating $f_t$ from MQI (Eq. 11) and using reference values for $f_t$ by the Italian code, which depend on the masonry typology.

For walls that fail in shear, the Turnšek–Čačovič criterion leads also to a more accurate prediction of the failure mode than the Mohr–Coulomb criterion with $\mu = 0.4$. However, a similar accuracy can be achieved through the optimisation of the parameters of a Mohr–Coulomb criterion, such as the one in Eq. (8), among which the friction coefficient is the more relevant.

## 8 Drift capacity of stone masonry walls

The deformation capacity of walls is a key input parameter when applying displacement-based assessment methods to masonry buildings. Current code provisions do not differentiate between brick and stone masonry when specifying the drift capacity of walls (Petry and Beyer 2014a). EC8-3 (CEN 2005a) limits its application to concrete and brick masonry, but in engineering practice the values given in EC8-3 are often also applied to stone masonry. The objective of this section is to derive drift capacities for stone masonry walls, to identify parameters that influence the drift capacities at different limit states and to provide the input data that is required for a probabilistic seismic assessment of stone masonry structures. In addition, two simple drift capacity models for stone masonry are put forward, which are suitable for implementation in engineering practice.

It was shown in Sect. 4 that monotonic tests lead to significantly larger drift capacities than cyclic tests. Since drift capacity values are typically used in conjunction with seismic assessments, only cyclic tests are considered in the following. Disregarded are also tests on walls that were injected or repaired as well as all tests that did not pass the quality check. In total, 67 test were considered of which 2 belonged to masonry typology A, 8 to B, 19 to C, 6 to D, 20 to E and 12 to E1 (Fig. 15a). The drift capacities are evaluated for the six
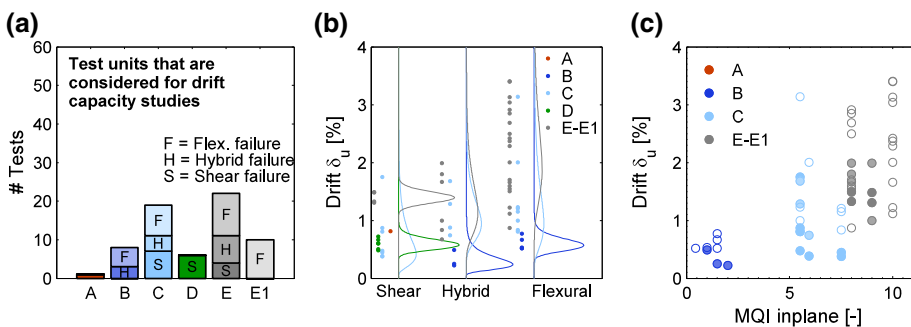


**Fig. 15** Distribution of test units considered for drift capacity studies (**a**). Ultimate drift capacity $\delta_u$ as a function of the failure mode (**b**), and the Masonry Quality Index for in-plane loading (**c**). *Solid markers* represent walls failing in shear of a hybrid mode; *empty markers* walls failing in flexure

element limit states introduced in Sect. 1: (1) the drift at the onset of cracking $\delta_{cr}$, (2), the drift at yield $\delta_y$, (3) the drift at maximum force $\delta_{max}$, (4) the drift at the limit state "Significant Damage" $\delta_{SD} = \min(3\delta_{cr}, \delta_{max})$ (5) the drift at ultimate limit state (20% strength drop) $\delta_u$, (6) the drift at collapse (50% strength drop) $\delta_c$. With the exception of the drift at the onset of cracking, the drift capacities are determined from the force–displacement envelope and its bilinear approximation. The drift at the onset of cracking is based on observations reported in the reference document but is not available for all tests. Note that the definition of onset of cracking differed between test campaigns. Some researchers distinguish between the appearance of flexural and shear cracks (e.g. Kržan and Bosiljkov 2012; Silva et al. 2014), others consider any type of crack (Vasconcelos 2005). Also, the minimum crack width that was detected probably differed between test series. The drift at the onset of cracking is therefore afflicted with an additional uncertainty. A detailed definition of the individual drift limits based on the envelopes in the positive and negative loading direction is included in the accompanying database.

## 8.1 Sensitivity of drift capacities at different limit states

The minimum and the maximum ultimate drift values of the 67 tests differ by more than a factor of 15 ($\delta_{u,min} = 0.22\%$ and $\delta_{u,max} = 3.4\%$). This is a rather significant ratio and the objective of this section is to identify factors that influence the drift capacity of stone masonry walls at different limit states. EC8-3 (CEN 2005a) assumes that the ultimate drift capacity depends on the failure mode. Figure 15b shows the distribution of the drift values for shear, hybrid and flexural failure. In general, shear and hybrid failures lead to a smaller drift capacity than flexural failures. Different trends are only observed when the sample size is very small (shear failure of Type E; hybrid failures Type C). To increase the size of the groups, the masonry typologies are regrouped as follows: the first group comprises types A–D and the second group types E and E1. Table 10 summarises for these two groups the median drift capacities and coefficients of variations for all considered limit states. Shear and hybrid failure modes lead to similar drift capacities and coefficients of variations. This finding suggests that it is not necessary to distinguish between shear and hybrid failure modes and in the remainder of this section drift capacities obtained from hybrid failure modes are counted towards shear failures.

One might expect that the drift capacity is positively correlated with the Masonry Quality Index and this is indeed confirmed by Fig. 15c. However, as shown by Fig. 4i, the axial load ratio also correlates strongly with the Masonry Quality Index (the larger the Masonry Quality Index, the smaller the axial load ratio that was applied in the test). Based on the current database it is therefore not possible to identify whether the drift capacity depends on the Masonry Quality Index or the axial load ratio or both. For other masonry typologies, it was already shown that the drift capacity decreases with increasing axial load ratio (e.g. Petry and Beyer 2014a; Rosti et al. 2016). For this reason, we investigate in the following the influence of the axial load ratio on the drift capacity of stone masonry walls at different limit states. Note that photos of the test units of typology D (Faella et al. 1992) were not available and therefore the Masonry Quality Index could not be determined.

Figure 16 shows the influence of the axial load ratio on the drift capacities for the different limit states. The drift $\delta_{cr}$ at the onset of cracking is relatively independent of the axial load ratio and of the masonry typology; for most walls the drift at the onset of cracking is between 0.1 and 0.3%. Only for some walls of typology E and E1, the drift at the onset of cracking is significantly larger. Drift capacities of all limit states tend to reduce with the axial load ratio but this trend is particularly evident for $\delta_y$, $\delta_{max}$ and $\delta_u$.

**Table 10** Median drift capacities and coefficients of variations for different limit states and masonry typologies

| | Number of test units per group | | Drift capacity (%) | | CoV | |
|---|---|---|---|---|---|---|
| | Shear failure | Flexural failure | Shear failure | Flexural failure | Shear failure | Flexural failure |
| Drift at the onset of cracking $\delta_{cr}$ | | | | | | |
| A–D | 10 | 12 | 0.15[b] | 0.25 | 0.35 | 0.20 |
| E, E1 | 11 | 21 | 0.25 | 0.15 | 0.55 | 0.65 |
| All | 21 | 33 | 0.15 | 0.15 | 0.75 | 0.55 |
| Drift at yield $\delta_y$ | | | | | | |
| A–D | 21 | 12[a] | 0.10 | 0.25 | 0.75 | 0.60 |
| E, E1 | 11 | 21 | 0.45 | 0.35 | 0.55 | 0.30 |
| All | 32 | 33 | 0.25 | 0.30 | 0.85 | 0.45 |
| Drift at "Significant Damage" LS $\delta_{SD}$ | | | | | | |
| A–D | 21 | 13 | 0.30 | 0.55 | 0.50 | 0.35 |
| E, E1 | 11 | 21 | 0.65 | 0.45 | 0.55 | 0.65 |
| All | 32 | 34 | 0.40 | 0.45 | 0.80 | 0.55 |
| Drift at maximum force $\delta_{max}$ | | | | | | |
| A–D | 21 | 13 | 0.30 | 0.65 | 0.75 | 0.65 |
| E, E1 | 11 | 21 | 1.00 | 1.95 | 0.40 | 0.45 |
| All | 32 | 34 | 0.45 | 1.05 | 0.75 | 0.65 |
| Drift at ultimate LS (20% drop in force) $\delta_u$ | | | | | | |
| A–D | 21 | 13 | 0.60 | 0.85 | 0.55 | 0.65 |
| E, E1 | 11 | 21 | 1.50 | 2.35 | 0.30 | 0.35 |
| All | 32 | 34 | 0.80 | 1.65 | 0.55 | 0.55 |
| Drift at collapse (50% drop in force) $\delta_c$ | | | | | | |
| A–D | 3 | 4 | 0.50[3] | 0.75[c] | 0.35 | 0.30 |
| E, E1 | 0 | 0 | – | – | – | – |
| All | 3 | 4 | 0.50[c] | 0.75[c] | 0.35 | 0.30 |

Drift capacities and CoVs are rounded to the nearest 0.05; shear failure comprises shear and hybrid failures

[a] For Test ID = 33 only $\delta_{max}$ and $\delta_u$ but not the entire force-drift envelope were available. Therefore $\delta_y$ could not be determined

[b] The drift at the onset of cracking was only available for 10 out of the 21 tests that failed in shear. The 10 tests led in average to larger yield drifts than the 21 tests and this is why the median value of $\delta_{cr}$ is larger than the median value of $\delta_y$ for walls failing in shear. For the 10 tests, for which $\delta_{cr}$ is known, the median yield drift was 0.30%, i.e., twice the drift at the onset of a cracking. For a median yield drift of 0.10%, it is therefore recommended to assume $\delta_{cr} = 0.05\%$

[c] The collapse drift was only available for 7 out of the 66 tests, for which $\delta_u$ could be determined. The 7 tests led in average to smaller drift capacities than the 66 tests and this is why the median value of $\delta_c$ is smaller than the median value of $\delta_u$. It is recommended to assume that $\delta_c/\delta_u = 1.1$ (Fig. 18d)

Figure 17a, b show the trends of the ultimate drift capacity with axial load ratio, if $\delta_u$ is normalised by $H_0/L$ (CEN 2005a) and by $H_0/H$ (Pfyl-Lang et al. 2011), respectively. The clearest trend with axial load ratio is obtained for $\delta_u L/H_0$. For brick masonry, it was further shown that the drift capacity decreases with the wall size (Petry and Beyer 2014a). For stone masonry walls, as for brick masonry, no test series investigated the effect of size on the drift capacity systematically. Figure 17c show the drift capacity of the walls contained
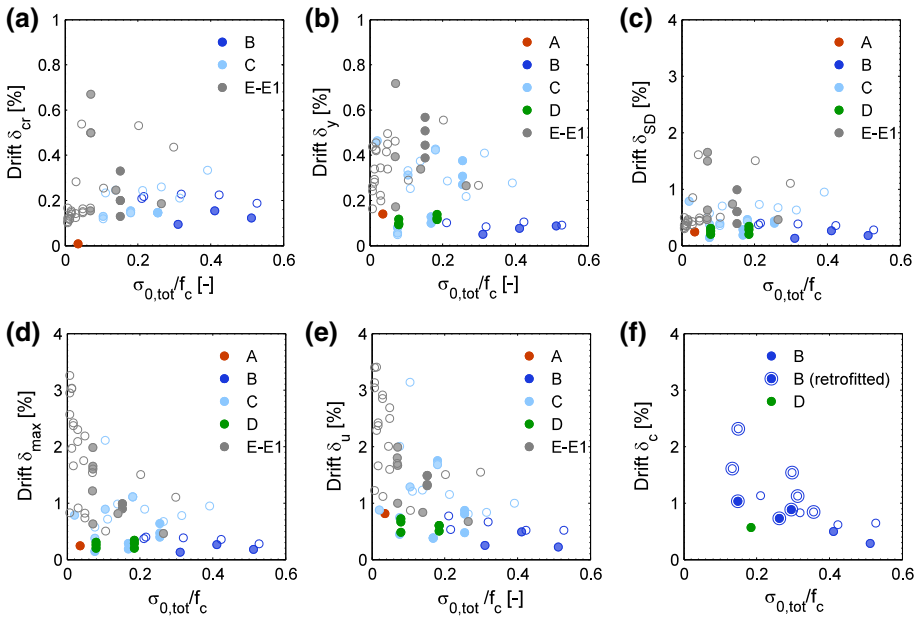
**Fig. 16** Influence of the axial load ratio on the drift capacity at different limit states: **a** drift at the onset of cracking $\delta_{cr}$; **b** drift at yield $\delta_y$; **c** drift at maximum force $\delta_{max}$; **d** drift limit "Significant Damage" $\delta_{SD} = \min(3\ \delta_{cr}, \delta_{max})$; **e** drift at ultimate LS $\delta_u$; **f** drift at collapse $\delta_c$. *Solid markers* represent walls failing in shear of a hybrid mode; *empty markers* walls failing in flexure. *Note*: The scale of the y-axis of plot **a** and **b** is different from those in plots **c–f**

in this database as a function of the wall height. Although the drift values tend to decrease with wall height, the trend for a single masonry typology is not clear. One reason why the size effect might be less important for stone masonry walls than for brick masonry walls is the fact that the size of the stones can be relatively easily reduced while small-scale brick wall tests are typically conducted with full-size bricks.

Figure 18a shows the displacement ductility $\mu = \delta_u/\delta_y$ as a function of the axial load ratio. The displacement ductilities vary between $\mu = 1.5$–$13.4$ for shear and hybrid failures and between $\mu = 2.0$–$41.5$ for flexural failures. The median displacement ductilities are $\mu = 4$ for shear and hybrid failures and $\mu = 6.5$ for flexural failures. The wide ranges highlight that displacement ductility is not a suitable parameter for characterising the deformation capacity of masonry walls. The ratio of the drift at the LS "Significant Damage" to the ultimate drift varies for shear/hybrid and flexural failure modes between $\delta_{SD}/\delta_u = 0.5$–$1.0$ (Fig. 18b). The median value is 0.5 and therefore smaller than what is assumed in EC8-3 ($\delta_{SD}/\delta_u = 3/4$). The ratio of 3/4 corresponds, however, rather well to the median ratios obtained for $\delta_{max}/\delta_u$ (Fig. 18c), for which a median value of 0.70 was obtained.

The limit state for which the least amount of data is available is the collapse limit state (Figs. 16f, 18d). Only seven tests were continued up to collapse; six walls originate from a single test series conducted by Silva et al. (2014). Out of these six tests, two failed in shear and four in flexure. The average collapse drift of these six tests is considerably smaller than the average ultimate drift of all 67 tests (Table 10). In order to increase the data base, the walls that were strengthened were also considered for the collapse limit state. Of the
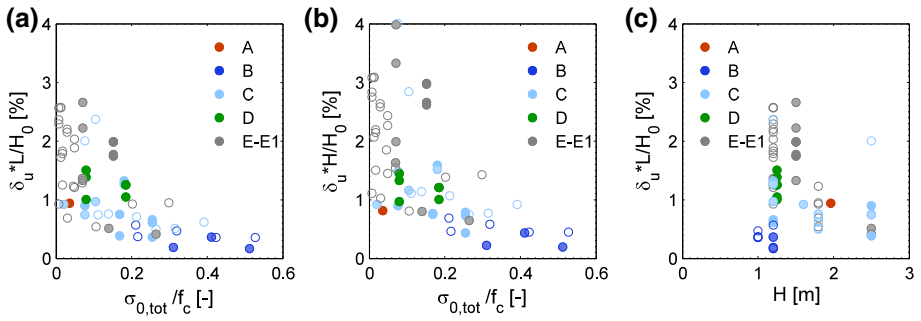
**Fig. 17** Ultimate drift capacity $\delta_u$: normalising the drift capacity by $L/H_0$ (**a**) and $H/H_0$ (**b**). Influence of the wall size on the drift capacity (**c**)



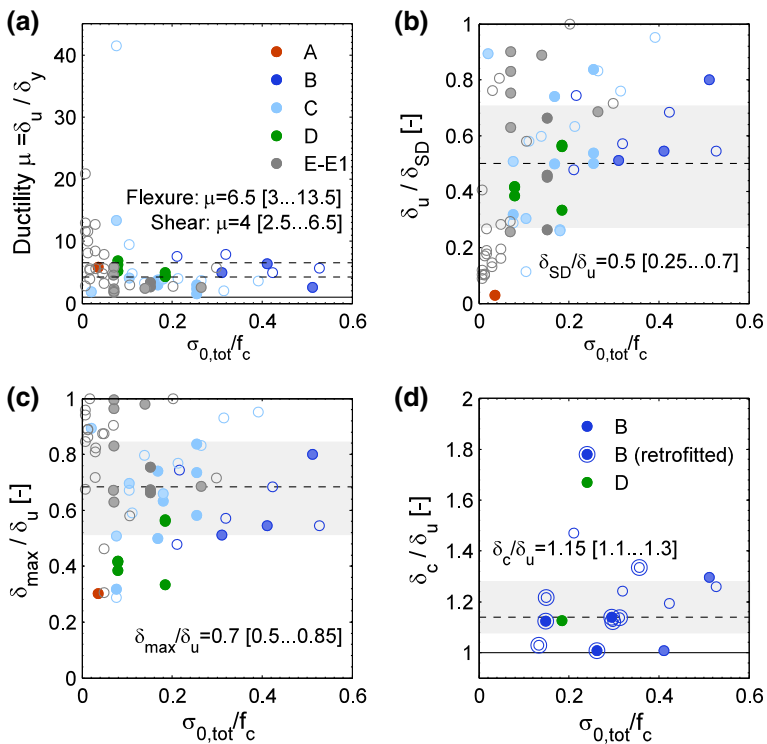**Fig. 18** Ratios of drifts at different limit states: **a** displacement ductility $\mu = \delta_u/\delta_y$; **b** ratio of ultimate drift $\delta_u$ to drift at the limit state "Significant Damage"; **c** ratio of collapse drift $\delta_c$ to ultimate drift $\delta_u$;. *Solid markers* represent walls failing in shear or a hybrid mode, *empty markers* walls failing in flexure. The *dashed line* represents the median value and the *shaded area* and the *range* corresponding to plus/minus one standard deviation

strengthened walls, eight walls were tested up to collapse; these tests were conducted by Silva et al. (2014) and Mazzon (2010). The drift at collapse decreases significantly with increasing axial load ratio (Fig. 16f). For walls failing in flexure the drift capacities at collapse are slightly larger than for walls failing in shear but the difference for the tests

reported here is not as large as one might have expected. Figure 18d shows the collapse drift to ultimate drift ratio for the 15 strengthened and unstrengthened walls that were tested up to collapse. This ratio seems to be rather independent of the axial load ratio and failure mode and its median value is $\delta_c/\delta_u = 1.15$.

## 8.2 Simple drift capacity models for engineering practice

The median drift values and CoVs given in Table 10 can be directly used in probabilistic assessments of stone masonry buildings. However, simpler models that can be summarised in fewer equations might often be more practical. The objective of this section is to propose two of such models. The first relates drift capacities to failure modes and masonry typology and the second relates drift capacity to axial load ratio, slenderness ratio and masonry typology. These models are inevitably less exact than the values of Table 10 and their derivation required some judgment in order to find a good balance between accuracy and simplicity.

The drift capacities are determined for the ultimate limit state ($\delta_u$). Based on the results presented in Fig. 18, drifts at all other limit states are expressed as a fraction of the drift at the ultimate limit state. Equations (12)–(17) summarise these relationships. The equations on the left represent median values and the equations on the right values that correspond to plus/minus one standard deviation assuming a lognormal distribution. One exception is the drift at the onset of cracking, for which a universal value of 0.20% is recommended, independent of the failure mode and masonry typology. The relationships between $\delta_u$ and the other drift limits apply independently of the chosen model for $\delta_u$. For the yield drift, two approaches are investigated. In the first approach, the yield drift is computed assuming a constant displacement ductility value which is assumed either as dependent on the failure mode or independent of the failure mode. In the second approach, the yield drift is computed from the predicted shear resistance and the predicted effective stiffness (Sects. 6, 7).

$$\delta_{cr} = 0.20\% \quad \delta_{cr} = [0.1\%\ldots0.35\%] \tag{12}$$

$$\text{Approach 1:} \quad \text{Flexural failure: } \delta_y = 1/6.5 \cdot \delta_u \quad \text{Flexural failure: } \delta_y = 1/[3.0\ldots13.5] \cdot \delta_u$$
$$\text{Shear failure: } \delta_y = 1/4 \cdot \delta_u \quad \text{Shear failure: } \delta_y = 1/[2.5\ldots6.5] \cdot \delta_u$$
$$\text{All failure modes: } \delta_y = 1/5 \cdot \delta_u \quad \text{All failure modes: } \delta_y = 1/[2.5\ldots10.5] \cdot \delta_u \tag{13}$$

$$\text{Approach 2:} \quad \delta_y = V_R/K_{eff} \tag{14}$$

$$\delta_{SD} = 0.5 \cdot \delta_u \quad \delta_{SD} = [0.25\ldots0.70] \cdot \delta_u \tag{15}$$

$$\delta_{max} = 0.7 \cdot \delta_u \quad \delta_{max} = [0.50\ldots0.85] \cdot \delta_u \tag{16}$$

$$\delta_c = 1.15 \cdot \delta_u \quad \delta_c = [1.10\ldots1.30] \cdot \delta_u \tag{17}$$

### 8.2.1 Model 1: drift capacity at ultimate limit state as a function of failure mode and masonry typology

In the absence of further test data, the masonry typologies are divided into two groups only (Group 1: A–D, Group 2: E–E1). The values of Table 11 are simplified so that the drift

**Table 11** Drift capacity model 1: recommended median drift capacities and coefficients of variations for $\delta_u$

| Masonry typology | Drift capacity (%) | | CoV | |
|---|---|---|---|---|
| | Shear failure | Flexural failure | Shear failure | Flexural failure |
| A–D | 0.60 | 0.90 | 0.60 | 0.60 |
| E, E1 | 1.50 | 2.25 | 0.40 | 0.40 |

capacity of walls failing in flexure corresponds to 1.5 times the drift capacity of walls failing in shear:

$$\delta_{u,flexure} = 1.5 \cdot \delta_{u,shear} \tag{18}$$

The drift capacity of the more regular masonry typologies (E–E1) is set to 2.5 times the drift capacity of masonry typologies A–D. The drift capacities at ultimate limit state for this first model and the corresponding CoVs are summarised in Table 11. The recommended CoVs for probabilistic assessments are 0.6 for masonry typologies A–D and 0.4 for masonry typologies E–E1. These recommended CoVs are approximate values of the CoVs reported in Table 13.

The drift capacities at the other limit states are computed using Eqs. (12)–(17). For a deterministic assessment, one typically uses a capacity that corresponds to a lower fractile value. Strength evaluations are typically based on the 5%-fractile value, which is referred to as the characteristic value. Current code estimates for drift capacities do not specify to which fractile value the drift capacity corresponds. If one assumes a lognormal distribution and the CoVs in Table 11, one obtains the ratios between fractile values and the median drift capacities as given in Table 12. For failure modes and masonry typologies for which the drift capacity can be predicted with a CoV of 0.6, the median drift capacity needs to be multiplied by 0.40 in order to obtain a drift capacity that corresponds to the 5%-fractile value. For a CoV of 0.4, 0.55 times the median drift capacity corresponds to the 5%-fractile value.

Figure 19 shows the distribution of the error between predicted and experimentally determined drift values for all six limit states. Table 13 summarises for the same values the median ratios of the predicted to experimental drifts and the CoV for the two groups of masonry typology (Group 1: A–D, Group 2: E–E1) and failure modes (shear/hybrid and flexure). The comparison assumes that the failure mode can be predicted correctly. One point was excluded from these plots and tables; this concerns the drift at the onset of cracking for Test ID 73 (cyclic in-situ test by Costa et al. 2011), which was reported as 0.008% and which is about 25 times smaller than drifts at the onset of cracking that were reported for other walls (Fig. 19a). As outlined at the beginning of Sect. 8, the drift values at the onset of cracking are not determined from the envelope curve but are taken from the test reports and are therefore not evaluated according to uniform criteria.

The displacement ductility values $\mu = \delta_u/\delta_y$ of the walls varied greatly (Sect. 8.1). This is reflected in the relatively large uncertainties (Table 13) when estimating the yield drift $\delta_y$ assuming constant ductility capacities for shear and flexural failures (Eq. (13)). However, due to the large uncertainty associated with the effective stiffness (Sect. 6), even larger CoVs are obtained when computing the yield drift from estimates of the shear strength and the effective stiffness (Eq. (14)). The distributions plotted in Fig. 19b show yield drift estimates that are computed assuming a fixed displacement ductility.

**Table 12** Ratios between fractile drift values and median drift values assuming that the drift capacities follow a lognormal distribution (ratios are rounded to the closest 0.05)

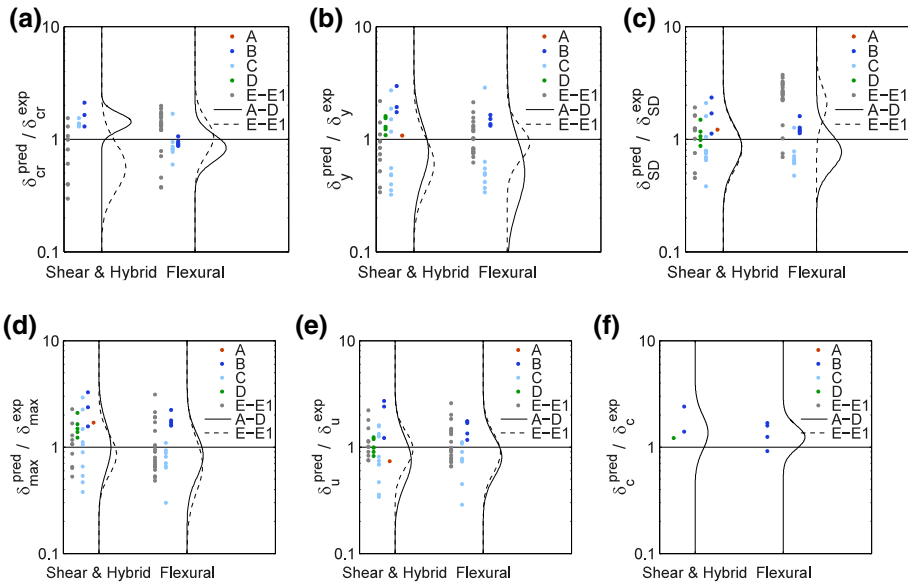| Fractile value (%) | CoV = 0.10 $\delta_{x\%}/\delta_{median}$ | CoV = 0.20 $\delta_{x\%}/\delta_{median}$ | CoV = 0.30 $\delta_{x\%}/\delta_{median}$ | CoV = 0.40 $\delta_{x\%}/\delta_{median}$ | CoV = 0.50 $\delta_{x\%}/\delta_{median}$ | CoV = 0.60 $\delta_{x\%}/\delta_{median}$ | CoV = 0.70 $\delta_{x\%}/\delta_{median}$ | CoV = 0.80 $\delta_{x\%}/\delta_{median}$ | CoV = 0.90 $\delta_{x\%}/\delta_{median}$ |
|---|---|---|---|---|---|---|---|---|---|
| 5 | 0.85 | 0.70 | 0.60 | 0.55 | 0.45 | 0.40 | 0.35 | 0.30 | 0.30 |
| 10 | 0.90 | 0.80 | 0.70 | 0.60 | 0.55 | 0.50 | 0.45 | 0.40 | 0.35 |
| 16 | 0.90 | 0.80 | 0.75 | 0.70 | 0.65 | 0.60 | 0.55 | 0.50 | 0.45 |
| 50 | 1 | 1 | 1 | 1 | 1 | 1 | 1 | 1 | 1 |

**Fig. 19** Drift capacity model 1: ratios of predicted to experimental drift capacities for the six different limit states. $\delta_{cr}$ (**a**), $\delta_y$ (**b**), $\delta_{SD}$ (**c**), $\delta_{max}$ (**d**), $\delta_u$ (**e**), $\delta_c$ (**f**)

**Table 13** Drift capacity model 1: median ratios and CoV for predicted to experimentally observed drift ratios ($\delta^{pred}/\delta^{exp}$)

| Masonry typology | A–D | | | | E–E1 | | | |
|---|---|---|---|---|---|---|---|---|
| | Shear failure | | Flexural failure | | Shear failure | | Flexural failure | |
| | Median ratio | CoV | Median ratio | CoV | Median ratio | CoV | Median ratio | CoV |
| $\delta_{cr}$ | 1.40 | 0.20 | 0.90 | 0.30 | 0.80 | 0.50 | 1.35 | 0.35 |
| $\delta_y$–const. duct. | 1.25 | 0.60 | 0.60 | 0.75 | 0.85 | 0.55 | 1.00 | 0.35 |
| $\delta_y = V_R/K_{eff}$ | 0.75 | 1.15 | 0.65 | 1.45 | 0.80 | 0.90 | 1.55 | 0.40 |
| $\delta_{SD}$ | 1.05 | 0.45 | 0.80 | 0.40 | 1.20 | 0.45 | 2.55 | 0.35 |
| $\delta_{max}$ | 1.50 | 0.55 | 0.95 | 0.50 | 1.05 | 0.45 | 0.80 | 0.65 |
| $\delta_u$ | 1.00 | 0.55 | 1.10 | 0.45 | 1.00 | 0.40 | 0.95 | 0.45 |
| $\delta_c$ | 1.40 | 0.40 | 1.40 | 0.25 | – | – | – | – |

Mean ratios capacities and CoVs are rounded to the nearest 0.05; shear failure comprises shear and hybrid failures

With the exception of the CoVs for $\delta_{cr}$ of masonry typology A-D, for which only a few data points are available, the CoVs of all limit states are rather similar and it is therefore recommended to use the CoVs that are given in Table 11 for the drift at the ultimate limit state as well for all other limit states. In some cases, the simple relationships of Eqs. (12)–(17) introduce a significant bias for a certain combination of failure mode and masonry typologies. Such a bias could of course be removed by assigning the coefficients of

Eqs. (12)–(17) on a case-to-case basis. However, for the sake of simplicity and considering the imperfect data base, a drift capacity model of such complexity does not seem justified.

### 8.2.2 Model 2: drift capacity at ultimate limit state as a function of axial load ratio, shear span and masonry typology

The second drift capacity model links the ultimate drift capacity to the axial load ratio and the shear span, which is normalised by the height. It follows therefore the drift form introduced by Pfyl-Lang et al. (2011) and applied in Petry and Beyer (2014a). Figure 20 plots the ultimate drift capacity that was normalised by min $(H, L)/H_0$ against the axial load ratio. The trendlines included in the figures represent median values of drifts that were obtained for bins of axial load ratio (bin width: 0.1). Equations (19) and (20) aim at approximating these trend lines. This method was used in order to account for the fact that the number of tests per bin varies significantly and tends to decrease with increasing axial load ratio. Therefore, the higher axial load ratios would be underrepresented if a simple linear fit was performed. For masonry typologies A–D, the following equation for the ultimate drift is proposed:

$$\delta_u = max \left( 1.5\% - 4\% \cdot \frac{\sigma_{0,tot}}{f_c}, 0.3\% \right) \cdot \frac{H_0}{min\,(H, L)} \tag{19}$$

The equations are applicable for $\sigma_{0,tot}/f_c \leq 0.6$ (Fig. 20b). For masonry typologies E and E1, the drift capacity is assumed to be 50% larger:

$$\delta_u = max \left( 2.25\% - 6\% \cdot \frac{\sigma_{0,tot}}{f_c}, 0.45\% \right) \cdot \frac{H_0}{min\,(H, L)} \tag{20}$$

Note that for masonry typologies E and E1, only the first branch of the equation could be validated since walls of such typologies were not tested for large axial load ratios.

For both groups and failure modes, the CoVs for the ultimate drifts lie for this second model between 0.40 and 0.60 (Table 14). The CoV are with this model even somewhat smaller for masonry typologies A–D than for masonry typologies E–E1. For the sake of simplicity and because clear trends are not recognisable, it is recommended to use a CoV for all masonry typologies and failure modes, if this second drift capacity model is applied. It is suggested to use CoV = 0.4 for $\delta_u$ and CoV = 0.6 for all other limit states. The
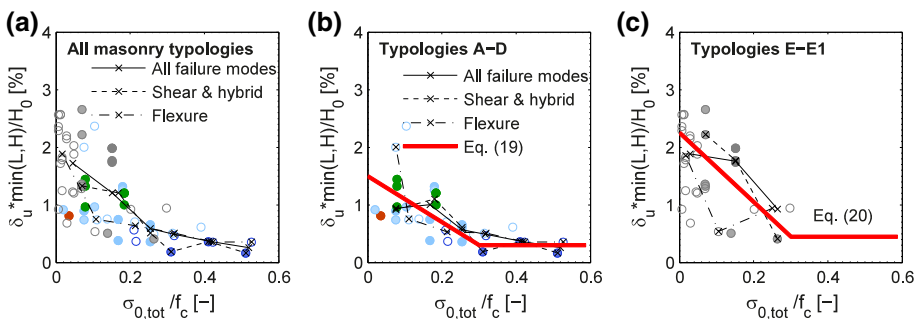


**Fig. 20** Drift capacity model 2: comparison of predicted and observed ultimate drift capacities for **a** all masonry typologies, **b** only masonry typology A–D, **c** only masonry typologies E–E1

**Table 14** Drift capacity model 2: median ratio and CoV for predicted to experimentally observed drift ratios ($\delta^{\text{pred}}/\delta^{\text{exp}}$)

| Masonry typology | A–D | | | | E–E1 | | | |
| --- | --- | --- | --- | --- | --- | --- | --- | --- |
| | Shear failure | | Flexural failure | | Shear failure | | Flexural failure | |
| | Median ratio | CoV | Median ratio | CoV | Median ratio | CoV | Median ratio | CoV |
| $\delta_{\text{cr}}^{\text{a}}$ | 1.40 | 0.20 | 0.90 | 0.30 | 0.80 | 0.50 | 1.35 | 0.35 |
| $\delta_{\text{y}}$–const. duct. | 0.90 | 0.80 | 0.85 | 1.05 | 0.45 | 0.70 | 1.55 | 0.45 |
| $\delta_{\text{y}} = V_{\text{R}}/K_{\text{eff}}^{\text{a}}$ | 0.75 | 1.15 | 0.65 | 1.45 | 0.80 | 0.90 | 1.55 | 0.40 |
| $\delta_{\text{SD}}$ | 1.10 | 0.45 | 0.75 | 0.55 | 0.85 | 0.65 | 3.1 | 0.40 |
| $\delta_{\text{max}}$ | 1.35 | 0.55 | 0.85 | 0.45 | 0.70 | 0.50 | 0.85 | 0.65 |
| $\delta_{\text{u}}$ | 1.10 | 0.40 | 0.85 | 0.40 | 0.75 | 0.60 | 1.1 | 0.50 |
| $\delta_{\text{c}}$ | 0.95 | 0.40 | 0.80 | 0.15 | – | – | – | – |

Median ratios capacities and CoVs are rounded to the nearest 0.05; shear failure comprises shear and hybrid failures

[a] Same values as for Model 1

distribution of the error between the predicted and experimentally determined drift values for the second model is shown in Fig. 21.

### 8.2.3 Comparison of different drift capacity models

The two models yield rather similar CoVs for the ultimate drift capacity (Model 1: 0.40–0.55; Model 2: 0.40–0.60). The error of Model 1 is expected to increase, if the
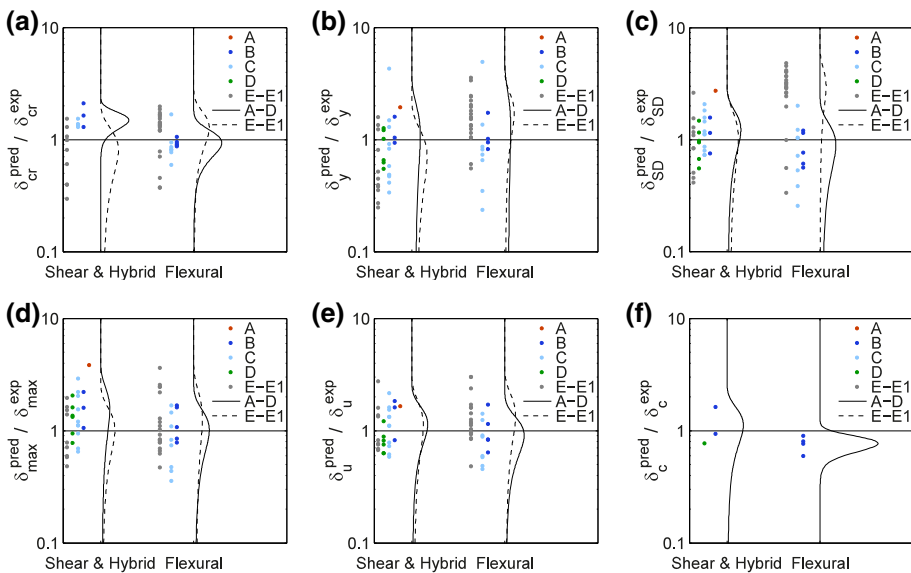


**Fig. 21** Drift capacity model 2: ratios of predicted to experimental drift capacities for the six different limit states. $\delta_{\text{cr}}$ (**a**), $\delta_{\text{y}}$ (**b**), $\delta_{\text{SD}}$ (**c**), $\delta_{\text{max}}$ (**d**), $\delta_{\text{u}}$ (**e**), $\delta_{\text{c}}$ (**f**)

predicted rather than the observed failure is used. The CoVs related to the ultimate deformation capacities of 0.40–0.60 might seem rather large. However, these CoVs are in fact similar to CoVs obtained for deformation capacities of reinforced concrete elements. Grammatikou et al. (2015) reported for reinforced concrete walls CoVs of 0.30 for the yield drift and between 0.30 and 0.50 for the ultimate drift, depending on the model used and the cross section of the wall. For reinforced concrete walls, the smallest CoVs were obtained with empirical models fitted to the data set and the largest CoVs with plastic hinge models (Grammatikou et al. 2015). More advanced analytical models for shear-critical reinforced concrete walls predict the ultimate drift capacity, however, with CoVs of less than 0.20 (e.g. Mihaylov et al. 2016). Similar CoVs for ultimate drift capacities are, however, also reached for clay brick masonry walls failing in shear or flexure if the drift capacity is predicted by an advanced analytical model (Petry and Beyer 2015; Wilding and Beyer 2017). Analytical models have therefore the potential to reduce the uncertainty related to the prediction of drift capacities and it is recommended to pursue in the future the development of such models for stone masonry walls. The reduction of the uncertainty is of course limited by the aleatoric variability, which—based on the limited data available— can be estimated to result in a CoV of 0.30 for the ultimate drift capacity (Table 3).

# 9 Summary and conclusions

The application of displacement-based assessment procedures requires robust estimates of the deformation capacity of every structural element. Eurocode 8, Part 3 [EC8-3, CEN (2005a)] as well as many other codes worldwide do not provide drift capacities specific to stone masonry walls. The objective of this project was to fill this gap and investigate specifically the drift capacity of stone masonry walls. In addition, the work aimed at providing input not only for the assessment of the ultimate limit state but for a large range of limit states ranging from the onset of cracking to the collapse of the wall. In view of probabilistic assessments, it was further the objective to provide next to median estimates also a measure of the confidence with which this quantity can be predicted. For this purpose, coefficients of variation (CoVs) were determined.

The work is based on a database of 123 shear–compression tests on stone masonry walls, which have been collected from 16 test campaigns documented in the literature; the database is made publically available. Based on these tests, stiffness, strength and deformation capacity were evaluated. The experimentally obtained values were compared to existing estimates and new or improved expressions proposed when this was indicated. More specifically, expressions for the following quantities as well as the corresponding CoVs were put forward (see summary in Table 15):

- *Stiffness* New expression for the effective E-modulus for the use in conjunction with a Timoshenko beam element model. Two types of expressions are proposed: (1) Median values and CoVs for the effective E-modulus for each masonry typology. (2) A more refined expression that accounts for the masonry typology, the compressive strength and the axial load ratio.
- *Strength* New values for the friction coefficient (Mohr–Coulomb criterion) and the tensile strength (Turnšek–Čačovič criterion). The values account for differences in stone masonry typologies.
- *Drift capacity values for six limit states* Two simple drift capacity models for the ultimate limit state and relationships between other limit state and $\delta_u$. The drift capacity

**Table 15** Summary of proposed median values and coefficients of variations for stone masonry assessment
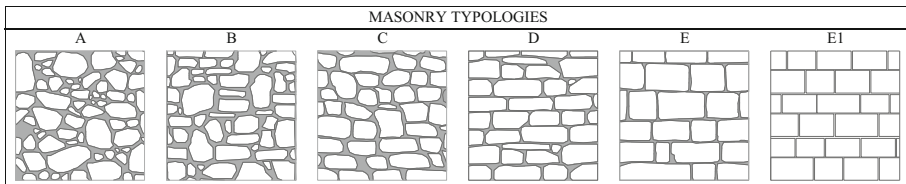
| MASONRY TYPOLOGIES | | | | | |
|---|---|---|---|---|---|
| A | B | C | D | E | E1 |



| FORCE CAPACITY | | A | B | C | D | E-E1 |
|---|---|---|---|---|---|---|
| Flexure: $V_{fl} = \frac{L^2 t}{2H_0}\sigma_0\left(1 - 1.15\frac{\sigma_0}{f_c}\right)$, $f_c$ from (1) | 1. $f_c$, [MPa] [1] | 1.40 | 2.50 | 3.20 | 1.90 | 7.00 |
| | CoV [1] | 0.30 | 0.20 | 0.19 | 0.27 | 0.14 |
| Shear: $V_{sh} = \frac{Lt}{b}f_t\sqrt{1+\frac{\sigma_0}{f_t}}$ | 2. $f_t$ code [MPa] [1] | 0.039 | 0.065 | 0.098 | 0.053 | 0.158 |
| | CoV | 0.24 | 0.19 | 0.14 | 0.20 | 0.14 |
| $f_t \cong 0.015 + 0.006 \cdot MQI^{1.5}$, or from (3) | 3. $f_t$ exp. [MPa] | 0.045 | 0.045 | 0.110 | 0.050 | 0.130 |
| | CoV | 0.80 | 0.30 | 0.20 | 0.50 | 0.40 |
| If a Mohr Coulomb criterion is preferred: values and CoVs | 4. Friction coeff. | 0.45 | 0.20 | 0.25 | 0.25 | 0.30 |
| for the friction angle in (4), $c = 2\mu f_t$ | CoV | 0.20 | 0.15 | 0.15 | 0.10 | 0.10 |

[1] from MIT (2009); coefficient of variation derived from CNR (2013)

| EFFECTIVE STIFFNESS | | A | B | C | D | E-E1 |
|---|---|---|---|---|---|---|
| $E_{eff} \cong \left(\frac{E}{f_c}\right)_{ref} f_c \cdot \frac{\sigma_0/f_c}{0.30}$　　or from (1-2). | 1. $E_{eff}$, code [MPa] [1] | 430 | 610 | 870 | 540 | 1400 |
| | CoV [1] | 0.20 | 0.20 | 0.15 | 0.20 | 0.15 |
| | 2. $E_{eff}$, exp. [MPa] | 320 | (2240) | 900 | 430 | 500-650 |
| $K_{eff} = \frac{1}{\frac{H^3}{2E_{eff}I}\left(\frac{H_0}{H}-\frac{1}{3}\right)+\frac{6H}{5G_{eff}Lt}}$　　with $\frac{G_{eff}}{E_{eff}}=0.33$ | CoV | 0.50 | (0.25) | 0.40 | 0.40 | 0.50 |
| | 3. $(E/f_c)_{ref}$ | 400 | (700) | 300 | 250 | 200-250 |
| | CoV | 0.40 | 0.40 | 0.40 | 0.40 | 0.40 |

[1] from MIT (2009); coefficient of variation derived from CNR (2013)

| DISPLACEMENT CAPACITY | | | A-B-C-D | | E-E1 | |
|---|---|---|---|---|---|---|
| | | | Shear failure | Flexural failure | Shear failure | Flexural failure |
| Drift at cracking: $\delta_{cr} = 0.20\%$　Drift at SD limit state $\delta_{SD} = 0.50 \cdot \delta_u$ Yielding drift:　　　　　　Drift at max. force: $\delta_{max} = 0.70 \cdot \delta_u$ | Model 1: $\delta_u$ | | 0.60 | 0.90 | 1.50 | 2.25 |
| - shear $\delta_y = 1/4 \cdot \delta_u$　Drift at collapse $\delta_c = 1.15 \cdot \delta_u$ - flexure $\delta_y = 1/6.5 \cdot \delta_u$ | CoV | | 0.50 | 0.50 | 0.50 | 0.50 |

Ultimate drift:　- Model 1:　reference values from table

- Model 2:　$\delta_u = \max(1.5\% - 4\% \cdot \frac{\sigma_{0,tot}}{f_c}, 0.3\%) \cdot \frac{H_0}{\min(H,L)}$　(typologies A-B-C-D)

$\delta_u = \max(2.25\% - 6\% \cdot \frac{\sigma_{0,tot}}{f_c}, 0.3\%) \cdot \frac{H_0}{\min(H,L)}$　(typologies E-E1)

| ALEATORIC VARIABILITY | Suggested coefficients of variation | | | | | | |
|---|---|---|---|---|---|---|---|
| | $K_{eff}$ | $V_u$ | $\delta_{cr}$ | $\delta_y$ | $\delta_{SD}$ | $\delta_{max}$ | $\delta_u$ | $\delta_c$ |
| A-E1 | 0.20 | 0.10 | 0.10 | 0.20 | 0.30 | 0.30 | 0.30 | - |

models distinguish between two groups of stone masonry typologies (Group 1: A–D, Group 2: E–E1).

- *Aleatoric variability* Aleatoric variabilities of stiffness, strength and drift limits for stone masonry.
- *Effect of load history and light retrofit interventions* Factors accounting for the effect of load history (monotonic vs cyclic) and light retrofit interventions (mortar injections) on stiffness, strength and drift limits.

The following paragraphs discuss the main findings of this work and identify future research needs.

Typology:

- Following the classification in the Italian code, five typologies of stone masonry were distinguished, which account for the shape of the stones, the number of leaves and their connectivity as well as the stone properties. For regular dressed stone masonry (typology E), a sub-class E1 was introduced that comprises stone masonry walls of typology E with regular shape (ashlar) and dry joints. It was found that ashlar masonry with dry joints shows an increase in stiffness but have little influence on strength and deformation capacity.
- The current database is rather scarce with regard to tests on walls of masonry typology A and D. Due to its wide distribution in existing masonry buildings, further tests would be desirable, in particular, on walls of typology A.

Shear strength of stone masonry walls:

- From the three quantities needed to describe the bi-linear response curve of stone masonry walls (effective stiffness, strength and drift capacity), the strength of the masonry walls can be predicted with the largest confidence. However, the strength equations of the form given in EC8-3 do not predict the failure mode well. For about a quarter of the walls failing in shear, a flexural failure is predicted. To err with regard to the failure mode does often not result in a very large error with regard to the force estimate since shear and flexural capacity can be rather similar. However, it might lead to a considerable error in the drift capacity, if models are used that link the drift capacity to the failure mode (such as the one in EC8-3).
- EC8-3, which application is limited to concrete and brick masonry but in engineering practice often also applied to other masonry typologies, predicts the shear strength of masonry walls by a Mohr–Coulomb criterion assuming a friction coefficient of $\mu = 0.4$. The latter appears to be too large when applied to stone masonry and the shear strength is therefore often overestimated. Using regression analysis on the experimentally determined wall strengths, best estimates of friction coefficients are calculated for each masonry typology.
- Slightly smaller coefficients of variations are obtained if not a Mohr–Coulomb but a Turnšek–Čačovič criterion is used for predicting the shear strength. This criterion needs as input a tensile strength of the masonry. The Italian code (NTC 2008; MIT 2009) provides reference values, which predicted the shear strength of the walls in the database very well. However, the CoV which could be taken from the Italian code, assuming that the given range limits correspond to 16th and 84th percentiles, seems to be too low by a factor of approximately 2. Borri et al. (2015) proposed an expression for the tensile strength which includes the Masonry Quality Index. Regression analysis on the shear strength and Masonry Quality Index of the walls included in the database confirm the expression proposed by Borri et al. (2015).

Effective stiffness of stone masonry walls:

- Estimating the effective stiffness of stone masonry walls is considerably more challenging than estimating their strength and the CoVs of predicted to experimentally determined stiffness is for all masonry typologies approximately 2–3 times larger than the CoVs for the strength. The effective stiffness can, however, be predicted with a slightly better confidence than the elastic wall stiffness. The ratio of effective to elastic stiffness varies greatly but the median ratio is close to 0.5, which corresponds to the value recommended in EC8-3.

- Available experimental results suggest that shear deformations contribute significantly to the flexibility of the walls but direct evaluations of the effective shear stiffness from experimental results are scarce. If one assumes a ratio of the shear to the elastic modulus and applies a Timoshenko beam element model, one can back-calculate the effective E-modulus from the wall stiffness. It was found that this effective stiffness depends on the masonry typology, the compression strength and the axial load ratio, i.e., the larger the axial load ratio, the larger the stiffness. The effect of the axial load ratio on the stiffness is not accounted for by modelling recommendations in current codes such as EC8-3, which connect the E-modulus solely to the compression strength, but it has already been identified by other research groups (Vasconcelos 2005; Bosiljkov et al. 2005). A new analytical expression for the effective E-modulus, which accounts for masonry typology, compression strength and axial load ratio, is proposed.

- It was further investigated if results from material tests lead to an improved estimate of the wall stiffness. The considered material tests were compression tests and dynamic identification tests. Surprisingly none of these results led to an improved estimate of the horizontal wall stiffness. One reason could be that the material tests addressed the E-modulus (i.e. flexural deformations) while shear deformations might contribute significantly to the wall flexibility. Another reason could be that the applied Timoshenko beam model is not appropriate to describe the wall kinematics and therefore the E-moduli that yields the best prediction is not related to a mechanical property of the material.

Drift capacity of stone masonry walls

- For the analysis of the drift capacities, only the cyclic tests were considered. Comparing the results of a monotonic and a cyclic test that were carried out within one test series suggests that the deformation capacity of cyclic tests is approximately only half of the deformation capacity under monotonic loading; this ratio was also observed for brick masonry walls (Beyer et al. 2014). The available data set did not allow more advanced analyses of the effect of the load history on the drift capacity as the parameters describing the cyclic loading protocol (number of cycles, drift intervals, mean value, …) were not varied in any of the test campaigns.

- Six different drift limit states were considered; these are (1) the drift at the onset of cracking $\delta_{cr}$, (2), the drift at yield $\delta_y$, (3) the drift at maximum force $\delta_{max}$, (4) the drift at the limit state "Significant Damage" $\delta_{SD} = \min(3\delta_{cr}, \delta_{max})$, (5) the drift at ultimate limit state (20% strength drop) $\delta_u$, (6) the drift at collapse (50% strength drop) $\delta_c$. With the exception of the drift at the onset of cracking, all drift limits were determined from the envelope of the force–drift relationship or its bilinear approximation. The drift at the onset of cracking was, if available, taken from test reports. The drift for which the least information was available is the drift at collapse. Only a very few tests were continued up to collapse and any estimates derived for this limit state need to be considered with great caution. To research this drift limit state further, additional experimental data is needed.

- For analysing the drift capacities, the tests were divided into two groups; the first group comprised walls of typologies A–D and the second walls of typologies E–E1. Given the rather large variability of the drift capacities and the limited number of tests available, a finer analysis did not seem warranted. Next to median values and CoVs for each group and failure mode, also two simple models for the ultimate drift capacity were proposed. The first connects the drift capacity to failure mode and masonry typology and follows therefore the approach of EC8-3 and many other current codes. The second one links

the drift capacity to masonry typology, axial load ratio and the factor $H_0/\min(H,L)$ where $H_0$ is the shear span and $H$ and $L$ the wall height and length, respectively. The two models lead to very similar CoVs. With the exception of the limit state at the onset of cracking, the drift capacities at the other limit states were expressed as a function of $\delta_u$. The drift at the onset of cracking was assigned a constant value ($\delta_{cr} = 0.20\%$).

- The current drift capacity model as well as the models proposed in this paper are empirical drift capacity models. In future tests, it would be desirable to also develop mechanical drift capacity models, which for brick masonry walls have already led to a considerable improvement in the drift capacity prediction (Sect. 8.2.3). For this purpose, wall tests with detailed measurements of the displacement fields are necessary. This would also allow to identify better the contributions of shear and flexural deformations to the total deformations and therefore pave the way for improved stiffness estimates. Furthermore, the effect of the stone pattern on the wall response should be investigated and first studies in this regard are currently underway.

Aleatoric variability

- The database contains 18 groups of replicate tests, which were used to estimate the aleatoric variability of stiffness, strength and drift capacities at different limit states. The strength varies in general the least (CoV = 0.1). Stiffness and drift capacities vary more (CoV = 0.2–0.3). Only the drift at the onset of cracking seems to lead to a smaller CoV (CoV = 0.1). None of the replicate tests was continued up to collapse and therefore the aleatoric variability could not be determined for $\delta_c$. From the available data, it was not possible to identify the effect of the masonry typology on the aleatoric variability. Also, all but one group of replicate tests were laboratory tests, which might not necessarily reproduce the aleatoric variability in real buildings. From the available data no significant difference between laboratory and in-situ tests could be identified. In future studies it would therefore be interesting to investigate the variation of aleatoric variability with masonry typology and to conduct further replicate in-situ tests.

Effect of retrofit interventions on drift capacity

- Also included in the database are tests with minor retrofit intervention (mortar injections or reinforcement through the wall thickness to improve the connection between the leaves). By comparing walls with mortar injections to their unstrengthened counterparts, the effect of the retrofit interventions could be identified. For stiffness and strength, such factors are already available in the Italian code (MIT 2009) and these were confirmed by the results obtained here. As a novelty, factors for the drift capacity were derived. The results showed that the ultimate drift capacity can increase by a factor of 3–6; the increase is particularly significant if the failure mode changes from shear to flexure. The experimental data on the effect of retrofit interventions is, however, still rather scarce and more data necessary. Mechanical drift capacity models, once they are available, might allow to predict the effect of retrofit interventions without testing all possible configurations.

# References

Almeida C, Guedes JP, Arêde A (2012) Shear and compression experimental behaviour of one leaf stone masonry walls. In: Proceedings of the 15th world conference on earthquake engineering. Lisbon, Portugal, pp 1–10

Almeida C, Arêde A, Guedes JP, Costa A (2014) Shear–compressive experimental behaviour of one-leaf stone masonry in north of Portugal. In: Second European conference on earthquake engineering and seismology. Istanbul, Turkey, pp 1–13

Angelillo M, Lourenço PB, Milani G (2014) Masonry behaviour and modelling. In: Angelillo M (ed) Mechanics of masonry structures. Springer, Vienna, pp 1–26

Benedetti D, Tomaževič M (1984) Sulla verifica sismica di costruzioni in muratura. Ing Sismica 1:9–16

Beyer K, Mangalathu S (2012) Review of strength models for masonry spandrels. Bull Earthq Eng 11:521–542. doi:10.1007/s10518-012-9394-3

Beyer K, Petry S, Tondelli M, Paparo A (2014) Towards displacement-based seismic design of modern unreinforced masonry structures. In: Ansal A (ed) Perspectives on European earthquake engineering and seismology. Springer International Publishing, pp 401–428. doi:10.1007/978-3-319-07118-3

Binda L, Cardani G, Saisi A (2009) Caratterizzazione sperimentale della qualità muraria. In: Proceedings of the conference "Anidis 2009". Italy, Bologna, pp 1–10

Borri A, De Maria A (2009) L'indice di qualità muraria (IQM): evoluzione e applicazione nell'ambito delle Norme Tecniche per le Costruzioni del 2008. In: Proceedings of the conference "Anidis 2009". Italy, Bologna, pp 1–27

Borri A, Corradi M, Vignoli A (2001) Il problema della valutazione della resistenza a taglio della muratura mediante prove sperimentali. In: Proceedings of the conference "Anidis 2001". Potenza–Matera, Italy, pp 1–11

Borri A, Paci G, De Maria A (2011) Resistenza a taglio delle murature: prove diagonali e correlazione con l'Indice di Qualità Muraria IQM. In: Proceedings of the conference "Anidis 2011". Bari, Italy, pp 1–10

Borri A, Castori G, Corradi M (2012) Evaluation of shear strength of masonry panels through different experimental analyses. In: 14th Structural faults and repair. Edinburgh, Scotland, pp 1–13

Borri A, Corradi M, Castori G, De Maria A (2015) A method for the analysis and classification of historic masonry. Bull Earthq Eng 13:2647–2665. doi:10.1007/s10518-015-9731-4

Bosiljkov VZ, Totoev YZ, Nichols JM (2005) Shear modulus and stiffness of brickwork masonry: an experimental perspective. Struct Eng Mech 20:21–43. doi:10.12989/sem.2005.20.1.021

Cardani G, Binda L (2015) Guidelines for the evaluation of the load-bearing masonry quality in built heritage. In: Toniolo L, Boriani M, Guidi G (eds) Built heritage: monitoring conservation management. Springer International Publishing, pp 127–139. doi:10.1007/978-3-319-08533-3

CEN (2005a) EN 1998-3: 2005 Eurocode 8: design of structures for earthquake resistance—part 3: assessment and retrofitting of buildings. Comité Européen de Normalisation, Brussels, Belgium

CEN (2005b) EN 1996-1-1:2005 Eurocode 6: design of masonry structures—part 1-1: common rules for reinforced and unreinforced masonry structures. Comité Européen de Normalisation, Brussels, Belgium

CNR (2013) DT 212/2013: Istruzioni per la valutazione affidabilistica della sicurezza sismica di edifici esistenti. Brussels, Belgium

Corradi M, Borri A, Castori G, Sisti R (2014) Shear strengthening of wall panels through jacketing with cement mortar reinforced by GFRP grids. Compos Part B Eng 64:33–42. doi:10.1016/j.compositesb.2014.03.022

Costa AA, Arêde A, Costa A, Oliveira CS (2011) In situ cyclic tests on existing stone masonry walls and strengthening solutions. Earthq Eng Struct Dyn 40:449–471. doi:10.1002/eqe.1046

Costa AA, Penna A, Arêde A, Costa A (2015) Simulation of masonry out-of-plane failure modes by multi-body dynamics. Earthq Eng Struct Dyn 44:2529–2549. doi:10.1002/eqe.2596

D'Ayala D, Speranza E (2003) Definition of collapse mechanisms and seismic vulnerability of historic masonry buildings. Earthq Spectra 19:479–509. doi:10.1193/1.1599896

Devaux M (2008) Seismic vulnerability of cultural heritage buildings in Switzerland. PhD thesis, EPFL, Lausanne, Switzerland

Doglioni F, Mirabella Roberti G, Bondanelli M (2009) Definizione della Linea di Minimo Tracciato come elemento per la qualifica dell'ingranamento nel piano e fuori dal piano, Prodotto finale Linea 1, progetto Reluis

Dolsek M (2009) Incremental dynamic analysis with consideration of modeling uncertainties. Earthq Eng Struct Dyn 38:805–825. doi:10.1002/eqe

Faella G, Manfredi G, Realfonzo R (1992) Cyclic behaviour of tuff masonry walls under horizontal loadings. In: 6th Canadian masonry symposium, Saskatoon, Canada, pp 1–11

Frumento S, Magenes G, Morandi P, Calvi GM (2009) Interpretation of experimental shear tests on clay brick masonry walls and evaluation of q-factors for seismic design. IUSS Press, Pavia

Grammatikou S, Biskinis D, Fardis MN (2015) Strength, deformation capacity and failure modes of RC walls under cyclic loading. Bull Earthq Eng 13:3277–3300. doi:10.1007/s10518-015-9762-x

Grünthal G (1998) Macroseismic Scale 1992 (EMS-92). European seismological commission, sub commission on engineering seismology, working group macroseismic

Kržan M, Bosiljkov V (2012) Results of laboratory and in situ tests on masonry properties and tables with mechanical parameters to be adopted in numerical modelling, PERPETUATE Project, Deliverable D15, www.perpetuate.eu

Kržan M, Gostič S, Cattari S, Bosiljkov V (2015) Acquiring reference parameters of masonry for the structural performance analysis of historical buildings. Bull Earthq Eng 13:203–236. doi:10.1007/s10518-014-9686-x

Lourenço PB (1996) Computational strategies for masonry structures. PhD thesis, Delft Univesity Press, Netherlands

Lourenço PB, Oliveira DV, Roca P, Orduña A (2005) Dry joint stone masonry walls subjected to in-plane combined loading. J Struct Eng 131:1665–1673. doi:10.1061/(ASCE)0733-9445(2005)131:11(1665)

Magenes G, Calvi GM (1997) In-plane seismic response of brick masonry walls. Earthq Eng Struct Dyn 26:1091–1112. doi:10.1002/(SICI)1096-9845(199711)26:11<1091:AID-EQE693>3.0.CO;2-6

Magenes G, Penna A, Galasco A, da Paré M (2010) In-plane cyclic shear tests of undressed double leaf stone masonry panels. In: 8th international masonry conference, Dresden, Germany, pp 1–10

Marcari G, Manfredi G, Prota A, Pecce M (2007) In-plane shear performance of masonry panels strengthened with FRP. Compos Part B Eng 38:887–901. doi:10.1016/j.compositesb.2006.11.004

Mazzon N (2010) Influence of grout injection on the dynamic behaviour of stone masonry buildings. PhD thesis, University of Padova, Italy

Mergos PE, Beyer K (2014) Loading protocols for European regions of low to moderate seismicity. Bull Earthq Eng 12:2507–2530. doi:10.1007/s10518-014-9603-3

Mihaylov BI, Hannewald P, Beyer K (2016) Three-parameter kinematic theory for shear-dominated reinforced concrete walls. J Struct Eng 142:4016041. doi:10.1061/(ASCE)ST.1943-541X.0001489

MIT (2009) Ministry of Infrastructures and Transportation, Circ. N. 617 of 2/2/2009: Istruzioni per l'applicazione delle nuove norme tecniche per le costruzioni di cui al Decreto Ministeriale 14 Gennaio 2008. Italy

NTC (2008) Decreto Ministeriale 14/1/2008: Norme tecniche per le costruzioni. Ministry of Infrastructures and Transportations, G.U.S.O. n.30 on 4/2/2008; Italy

Oliveira DV (2003) Experimental and numerical analysis of blocky masonry structures under cyclic loading. PhD thesis, University of Minho, Portugal

Penna A (2015) Seismic assessment of existing and strengthened stone-masonry buildings: critical issues and possible strategies. Bull Earthq Eng 13:1051–1071. doi:10.1007/s10518-014-9659-0

Petry S, Beyer K (2014a) Influence of boundary conditions and size effect on the drift capacity of URM walls. Eng Struct 65:76–88. doi:10.1016/j.engstruct.2014.01.048

Petry S, Beyer K (2014b) Limit states of modern unreinforced clay brick masonry walls subjected to in-plane loading. Bull Earthq Eng 1073–1095. doi:10.5281/zenodo.8443

Petry S, Beyer K (2015) Force–displacement response of in-plane-loaded URM walls with a dominating flexural mode. Earthq Eng Struct Dyn 44:2551–2573. doi:10.1002/eqe.2597

Pfyl-Lang K, Braune F, Lestuzzi P (2011) SIA D0237: Beurteilung von Mauerwerksgebäuden bezüglich Erdbeben (SIA D 0237: Evaluation de la sécurité parasismique des bâtiments en maçonnerie). Zürich, Switzerland

Pinho FFS, Lúcio VJG, Baião MFC (2012) Rubble stone masonry walls in Portugal strengthened with reinforced micro-concrete layers. Bull Earthq Eng 10:161–180. doi:10.1007/s10518-011-9280-4

Rosti A, Penna A, Rota M, Magenes G (2016) In-plane cyclic response of low-density AAC URM walls. Mater Struct 49:4785–4798. doi:10.1617/s11527-016-0825-5

Rota M, Penna A, Magenes G, Magenes G (2014) A framework for the seismic assessment of existing masonry buildings accounting for different sources of uncertainty. Earthq Eng Struct Dyn 43:1045–1066

Silva B (2012) Diagnosis and strengthening of historical masonry structures: numerical and experimental analysis. PhD thesis, University of Padova, Italy

Silva B, Guedes JM, Arêde A, Costa A (2012) Calibration and application of a continuum damage model on the simulation of stone masonry structures: Gondar church as a case study. Bull Earthq Eng 10:211–234. doi:10.1007/s10518-010-9216-4

Silva B, Dalla Benetta M, Da Porto F, Modena C (2014) Experimental assessment of in-plane behaviour of three-leaf stone masonry walls. Constr Build Mater 53:149–161. doi:10.1016/j.conbuildmat.2013.11.084

Tomaževič M (1999) Earthquake-resistant design of masonry buildings. Imperial College Press, London

Tomaževič M (2007) Damage as a measure for earthquake-resistant design of masonry structures: Slovenian experience. Can J Civ Eng 34:1403–1412. doi:10.1139/L07-128

Turnšek V, Čačovič F (1971) Some experimental results on the strength of brick masonry walls. In: Proceedings of the 2nd international brick masonry conference. Stoke-on-Trent, England, pp 149–156

Vamvatsikos D, Fragiadakis M (2010) Incremental dynamic analysis for estimating seismic performance sensitivity and uncertainty. Earthq Eng Struct Dyn 141–163. doi:10.1002/eqe

Vasconcelos G (2005) Experimental investigations on the mechanics of stone masonry: characterization of granites and behavior of ancient masonry shear walls. PhD thesis, University of Minho, Portugal

Vasconcelos G, Lourenço PB (2009) In-Plane experimental behavior of stone masonry walls under cyclic loading. J Struct Eng 135:1269–1277. doi:10.1061/(ASCE)ST.1943-541X.0000053

Wilding BV, Beyer K (2017) Force–displacement response of in-plane loaded unreinforced brick masonry walls: the critical diagonal crack model. Bull Earthq Eng 15:2201–2244. doi:10.1007/s10518-016-0049-7